

Article

New Cu(II), Cu(I) and Ag(I) Complexes of Phenoxy-Ketimine Schiff Base Ligands: Synthesis, Structures and Antibacterial Activity

Miriam Caviglia ¹ , Zhenzhen Li ^{1,2} , Carlo Santini ¹ , Jo' Del Gobbo ¹ , Cristina Cimorelli ¹ , Miao Du ^{2,*} ,
Alessandro Dolmella ^{3,*}  and Maura Pellei ^{1,*} 

- ¹ School of Science and Technology, Chemistry Division, University of Camerino, Via Madonna Delle Carceri (ChIP), 62032 Camerino, Italy; miriam.caviglia@unicam.it (M.C.); zhenzhen.li@unicam.it (Z.L.); carlo.santini@unicam.it (C.S.); jo.delgobbo@unicam.it (J.D.G.); cristina.cimorelli@unicam.it (C.C.)
² College of Material and Chemical Engineering, Institute of New Energy Science and Technology, Zhengzhou University of Light Industry, Zhengzhou 450001, China
³ Department of Pharmaceutical and Pharmacological Sciences, University of Padova, Via Marzolo 5, 35131 Padova, Italy
* Correspondence: dumiao@zzuli.edu.cn (M.D.); alessandro.dolmella@unipd.it (A.D.); maura.pellei@unicam.it (M.P.)

Abstract: Two phenoxy-ketimines ligands, 2-(1-(benzylimino)ethyl)phenol (HL^{BSMe}) and 2-((benzylimino)(phenyl)methyl)phenol (HL^{BSPH}), were synthesized and used as supporting ligands of new copper(II), copper(I), and silver(I) complexes. In order to confer different solubility properties to the metal complexes and to stabilize Cu and Ag in their +1 oxidation state, the lipophilic triphenylphosphine (PPh₃) and the hydrophilic 1,3,5-triaza-7-phosphaadamantane (PTA) were selected as co-ligands in the syntheses of the Cu(I) and Ag(I) complexes. All compounds were characterized by CHN analysis, NMR, FT-IR spectroscopy, and electrospray ionization mass spectrometry (ESI-MS); the molecular structure of the copper(II) complex [Cu(L^{BSPH})₂] was also determined by single-crystal X-ray diffraction. Finally, the antibacterial activity of the metal complexes, the Schiff base ligands and phosphane co-ligands, were assessed by determining the minimum inhibitory concentration (MIC) and minimum bactericidal concentration (MBC) against Gram-negative (*Escherichia coli*) and Gram-positive bacteria (*Staphylococcus aureus*).

Keywords: silver; copper; Schiff bases; phosphanes; single-crystal XRD; antibacterial activity



Academic Editor: Zbigniew Rozwadowski

Received: 3 April 2025

Revised: 17 April 2025

Accepted: 22 April 2025

Published: 24 April 2025

Citation: Caviglia, M.; Li, Z.; Santini, C.; Del Gobbo, J.; Cimorelli, C.; Du, M.; Dolmella, A.; Pellei, M. New Cu(II), Cu(I) and Ag(I) Complexes of Phenoxy-Ketimine Schiff Base Ligands: Synthesis, Structures and Antibacterial Activity. *Molecules* **2025**, *30*, 1893. <https://doi.org/10.3390/molecules30091893>

Copyright: © 2025 by the authors. Licensee MDPI, Basel, Switzerland. This article is an open access article distributed under the terms and conditions of the Creative Commons Attribution (CC BY) license (<https://creativecommons.org/licenses/by/4.0/>).

1. Introduction

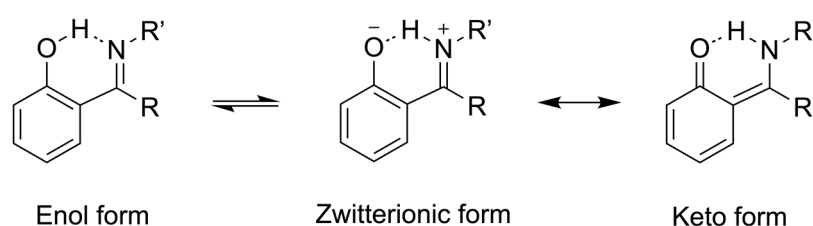
In recent years, the phenomenon of antibiotic resistance in hospitals, communities, and the environment has increasingly grown. Antibacterial resistance is a major global public health challenge, associated with an estimated 4.95 million deaths in 2019 [1,2]. Due to these developments, the World Health Organization (WHO) published the first list of drug-resistant bacterial priority pathogens classified as critical in 2017 [3]. Building on the 2017 edition, in 2024, the WHO published an updated list of drug-resistant bacteria posing the greatest threat to human health, aiming to guide the development of new treatments and strategies to prevent and mitigate the spread of antimicrobial resistance (AMR) [2]. Despite the current work, the global antibiotic pipeline is marked by limited innovation and limited global access to both new and existing treatments. This increase in antimicrobial resistance and the misuse of antimicrobials have led to the need to develop new antimicrobial compounds [4–8].

Medicinal inorganic chemistry offers possibilities for the design of therapeutic agents not readily available to organic compounds [7,9,10]. A successful strategy in antimicrobial chemotherapy has been the use of metallo-drugs, and this strategy has the potential to be used for treating multidrug-resistant infections more efficiently [4,11,12]. As a class of molecules, Schiff bases have been a topic of considerable interest, owing to their versatile metal chelating properties, and have been used to coordinate almost all metal ions [13–24]. Schiff bases and their metal complexes have been reported to exhibit a wide range of biological activities [15,25–34], including anticancer [35,36] and antimicrobial properties [37–45]. In most cases, the metallic derivatives of Schiff bases were found to exhibit higher antimicrobial activities than their parent ligands [27,46].

Numerous Schiff bases and their copper(II) derivatives have been reported to possess promising catalytic [47,48], anticancer [49–52], or biological properties [41,45,53–61] and have been successfully used as models in biological systems [62]. In particular, several Cu(II) complexes of *N,O*-donor Schiff base ligands were found to exhibit favorable antimicrobial activities [57,63–71].

Despite the enormous amount of work devoted to the synthesis and characterization of copper(II) Schiff bases complexes [65], there are relatively few reports devoted to the corresponding Cu(I) complexes, perhaps due to their tendency to undergo disproportionation to copper metal and copper(II) compounds in the absence of stabilizing co-ligands [72–74]. Schiff bases as chelating N-donors and phosphanes as P-donors were recently employed for the preparation of photoactive neutral [75,76] or cationic heteroleptic Cu(I) complexes [77–79]. On the other hand, in view of the wide spectra of antimicrobial activities against bacteria and fungi showed by silver(I) [80] and related to metal complexes [81–83], plenty of studies focused on the antimicrobial properties of silver(I) complexes with Schiff bases [84,85]. Recently, the Schiff bases Cu(I) and Ag(I) complexes incorporating phosphanes as co-ligands have awakened a new interest towards their biological properties [86].

Among the various types of Schiff bases [87–96], the phenoxy-imines and phenoxy-ketimines are of particular interest. These 2-imidoylphenols can exist in tautomeric forms due to intramolecular H-bonding between the hydroxyl H-atom and the N-atom (Scheme 1) [97–99].



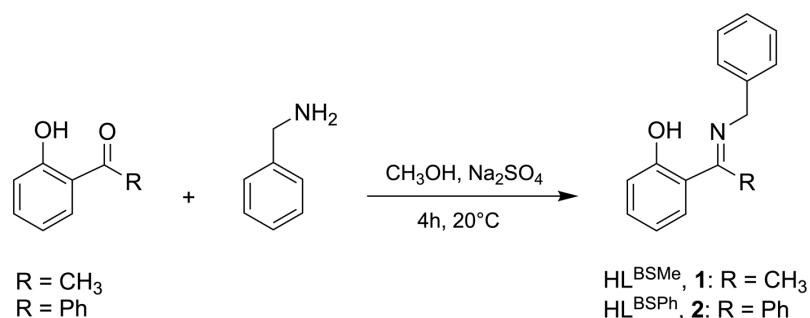
Scheme 1. Tautomerism of 2-imidoylphenols.

Depending on the extent of the interaction, complete transfer of the proton from the hydroxyl group to the nitrogen atom may occur, giving conversion of the molecular form (benzenoid, enol-type) into the quinoid, keto-type tautomer [98,100]. Zwitterionic species characterized by an intramolecular charge-separation are possible intermediates in the tautomerization process [99]. The replacement of the hydrogen atom by the methyl, ethyl, or phenyl substituents in the C-C(H)=N moiety in phenoxy-imines Schiff bases shortens the intramolecular hydrogen bonds in related phenoxy-ketimines [101].

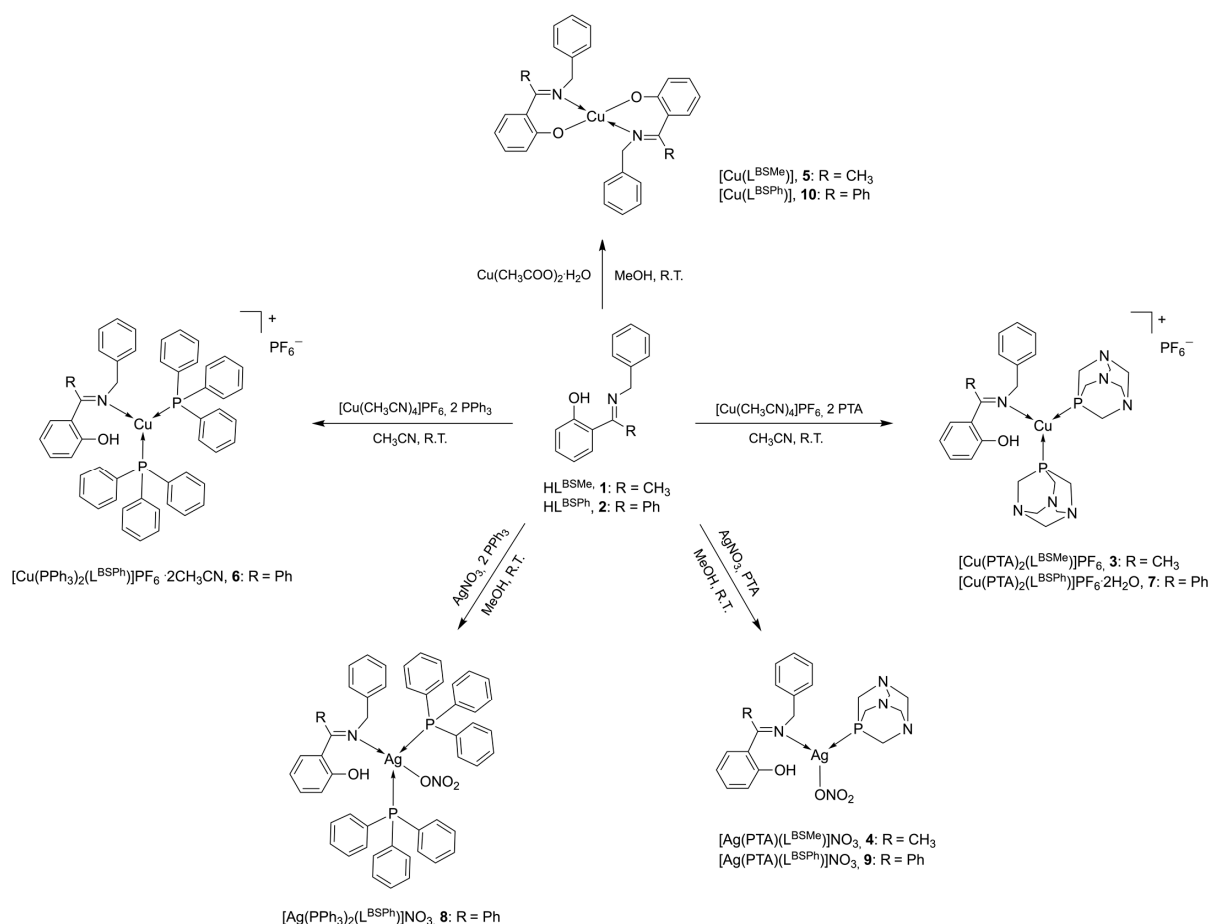
In recent years, metal complexes of *N,O*-bidentate phenoxy-ketimines Schiff base ligands have attracted much attention from researchers [47,48,102–110]. However, to our knowledge, copper(I)- and silver(I)-based complexes supported by *N,O*-bidentate

phenoxy-ketimines, including phenoxy-imines Schiff base ligands, remain an unexplored research field.

Therefore, as part of our continuous investigation on the chemical and biological properties of copper- and silver-containing coordination compounds [111–117], we report here the syntheses, characterization, and biological evaluation of new Cu(II), Cu(I), and Ag(I) complexes containing phosphanes and the phenoxy-ketimines ligands, 2-(1-(benzylimino)ethyl)phenol (HL^{BSMe}) (Oletimol), and 2-((benzylimino)(phenyl)methyl)phenol (HL^{B^{SP}h}) (Schemes 2 and 3). The ligands were selected to modify the steric and electronic properties of the resulting metal complexes using phenyl and methyl groups on the C-C(R)=N imino moiety, respectively. In designing the novel phenoxy-ketimines metal complexes, the lipophilic triphenylphosphine (PPh₃) and the hydrophilic 1,3,5-triaza-7-phosphaadamantane (PTA) were selected as co-ligands, in order to stabilize copper and silver in their +1 oxidation state and to confer different solubility properties to the corresponding metal complexes.



Scheme 2. Synthesis of HL^{BSMe} (**1**) and HL^{B^{SP}h} (**2**) ligands.



Scheme 3. Synthesis of compounds **3–10**.

The antimicrobial properties of the new copper and silver complexes as well as of the corresponding uncoordinated ligands and co-ligands were evaluated against Gram-negative (*Escherichia coli*) and Gram-positive (*Staphylococcus aureus*) bacteria. The antimicrobial data have been compared with the control antibiotic ciprofloxacin to assess their relative efficacy [66].

2. Results and Discussion

2.1. Synthesis and Characterization

The phenoxy-ketimines ligands HL^{BSMe} and HL^{BSPH} were prepared using a modified literature method [118–120], by the condensation reaction of the 2-acylphenols 2'–1-(2-hydroxyphenyl)ethan-1-one or (2-hydroxyphenyl)(phenyl)methanone, respectively, with stoichiometric amounts of benzylamine in methanol, and isolated as yellow solids in very good yield and high purity (Scheme 2).

The ligands were fully characterized by ¹H-NMR (Table S1), ¹³C-NMR, FT-IR spectroscopy, and ESI-MS spectrometry. Both 1,3,5-triaza-phosphaadamantane copper(I) complexes [Cu(HL^{BSMe})(PTA)₂PF₆] (3) and [Cu(HL^{BSPH})(PTA)₂PF₆·2H₂O] (7) were synthesized in CH₃CN using, as starting materials, the ligand HL^{BSMe} or HL^{BSPH}, the metal acceptor [Cu(CH₃CN)₄]PF₆, and the PTA co-ligands in the stoichiometric ratio 1:1:2, respectively (Scheme 3). Analogously, triphenylphosphine copper(I) complex [Cu(HL^{BSPH})(PPh₃)₂]PF₆·2CH₃CN (6) was synthesized in CH₃CN using, as starting material, the ligand HL^{BSPH}, the metal acceptor [Cu(CH₃CN)₄]PF₆, and the PPh₃ co-ligands in the stoichiometric ratio 1:1:2 (Scheme 3).

Elemental analyses and spectroscopic studies such as FT-IR, ¹H-, ³¹P-NMR, and ESI-MS confirm the stoichiometry of the synthesized complexes 3, 6, and 7. All the expected absorption bands were observed in the FT-IR spectra. The most characteristic feature of the complexation is the removal of the O···H···N hydrogen bond [101,121] and the presence of a very broad ν(OH) absorption band at about 3200 cm^{−1}. The complexes exhibit weak bands in the range of 2878–3070 cm^{−1} typical of C-H stretching. The strong absorptions at 1571–1618 cm^{−1} are due to the stretching of the aromatic and imine bonds (C=C and C=N), while very intense absorptions in the range of 831–832 cm^{−1} are attributable to the stretching of the PF₆[−] counterion. The ¹H-NMR spectra, recorded in CD₃CN for complexes 3, 6, and 7, confirm the stoichiometric ratio between the Schiff base ligand and phosphane co-ligands. They showed a single set of resonances for the skeletal ligands, indicating that the Schiff base ligand protons are equivalent. The signals of phenolic OH protons appeared as broad peaks in the range of 15.41–16.24 ppm, the signal of the CH₂Ph protons is visible at δ 4.55–4.83 ppm, while the signal of the ketimine methyl CH₃C=N proton for complex 3 appeared at δ 2.47 ppm, with a slight shift with respect to the signal of the free ligand due to the coordination to the copper acceptor. The aromatic hydrogens of ligand and triphenylphosphine co-ligands for [Cu(HL^{BSPH})(PPh₃)₂]PF₆·2CH₃CN (6) are detectable in the range of 6.71–7.69 ppm, while in the spectra of [Cu(HL^{BSMe})(PTA)₂]PF₆ (3) and [Cu(HL^{BSPH})(PTA)₂]PF₆·2H₂O (7) recorded in CD₃CN, the NCH₂P protons of PTA co-ligands are visible as singlets at δ 4.06–4.09 ppm and the related NCH₂N protons show characteristic AB quartets in the range of 4.52–4.60 ppm.

The ³¹P-NMR spectrum of [Cu(HL^{BSPH})(PPh₃)₂]PF₆·2CH₃CN (6) performed in CD₃CN gives a broad singlet peak at −0.30 ppm, downfield shifted with respect to the value of the free triphenylphosphine in the same solvent (δ = −4.85 ppm). Likewise, a broad singlet is visible in the spectra of the PTA complexes 3 and 7, recorded in CD₃CN, at −91.64 and −89.66 ppm, downfield shifted with respect to the value of the free PTA in CD₃CN (δ = −102.07 ppm). Moreover, the spectra of complexes 3, 6, and 7 show the distinctive septets due to the presence of the PF₆[−] counterion at about −144.60 ppm with J_{F–P} = 706 Hz. ¹H-

NMR and $^{31}\text{P}\{^1\text{H}\}$ -NMR data of complexes **3**, **6**, and **7** are summarized in Table S1. The ESI-MS study was performed by dissolving complexes **3**, **6**, and **7** in acetonitrile and recording the spectra in ion-positive and ion-negative modes. In the ESI-MS(+) spectrum of **3**, the major peak at m/z 445 can be attributed to the species $[\text{Cu}(\text{HL}^{\text{BSMe}})(\text{PTA})]^+$. Similarly, the ESI-MS(+) spectrum of **7** showed at m/z 507 the peak due to the species $[\text{Cu}(\text{HL}^{\text{BSPH}})(\text{PTA})]^+$, confirming the formation and the stability of the complexes.

The copper(II) complexes $[\text{Cu}(\text{L}^{\text{BSMe}})_2]$ (**5**) and $[\text{Cu}(\text{L}^{\text{BSPH}})_2]$ (**10**) were synthesized using the copper(II) acetate salt $\text{Cu}(\text{CH}_3\text{COO})_2$ and the ligands HL^{BSMe} and HL^{BSPH} , respectively, in the stoichiometric ratio 1:2 (Scheme 3). The reaction was performed in methanol at reflux for the synthesis of complex **5** and in acetonitrile at room temperature for the synthesis of **10**. Isolated complexes are air-stable, soluble in CH_3OH , CH_3CN , CH_2Cl_2 , CHCl_3 , and DMSO, and they have been characterized by means of FT-IR spectroscopy and ESI-MS spectrometry. Successful complexation was indicated by a slight shift of the imine bonds ($\nu(\text{C}=\text{N})$) in the IR spectra. In particular, the imine and aromatic bands in complexes **5** and **10** are observed at $1588\text{--}1597\text{ cm}^{-1}$ and $1569\text{--}1599\text{ cm}^{-1}$, respectively, whereas in the corresponding ligand precursors HL^{BSMe} and HL^{BSPH} , the bands appear at $1572\text{--}1610$ and $1563\text{--}1604\text{ cm}^{-1}$, respectively. The ESI-MS spectra of complexes **5** and **10** were performed in CH_3CN solution. In the ESI-MS(+) of complex **5**, peaks at m/z 287 and 329 are due to the species $[\text{Cu}(\text{L}^{\text{BSMe}})]^+$ and $[\text{Cu}(\text{L}^{\text{BSMe}}) + \text{CH}_3\text{CN}]^+$, respectively; the major peaks at m/z 511 and 576, respectively, are due to the adducts $[\text{Cu}(\text{L}^{\text{BSMe}})_2 + \text{H}]^+$ and $[\text{Cu}(\text{L}^{\text{BSMe}})_2 + \text{Na} + \text{CH}_3\text{CN}]^+$, respectively, confirming the presence of two ligands that coordinate copper. For complex **10**, signals at m/z 349 and 390 are attributable to the fragments $[\text{Cu}(\text{L}^{\text{BSPH}})]^+$ and $[\text{Cu}(\text{L}^{\text{BSPH}}) + \text{CH}_3\text{CN}]^+$.

The silver complexes $[\text{Ag}(\text{HL}^{\text{BSMe}})(\text{PTA})]\text{NO}_3$ (**4**) and $[\text{Ag}(\text{HL}^{\text{BSPH}})(\text{PTA})]\text{NO}_3$ (**9**) were synthesized by a treatment of AgNO_3 with one equivalent of 1,3,5-triaza-phosphadaamantane (PTA) and one equivalent of the corresponding HL^{BSMe} or HL^{BSPH} ligands in methanol and acetonitrile solution, respectively. Likewise, the triphenylphosphine silver(I) complex $[\text{Ag}(\text{HL}^{\text{BSPH}})(\text{PPh}_3)_2]\text{NO}_3$ (**8**) was synthesized in CH_3CN using as starting material the ligand HL^{BSPH} , the metal acceptor silver nitrate, and the PPh_3 co-ligands in the stoichiometric ratio 1:1:2. Isolated complexes are air-stable and have been characterized by means of ^1H -, ^{31}P -NMR and FT-IR spectroscopy, as well as ESI-MS spectrometry. In IR spectra, a slight shift of the imine bonds ($\nu(\text{C}=\text{N})$) was observed, indicating complexation. Complexes **4**, **8**, and **9** exhibit a series of bands in the $1479\text{--}1292\text{ cm}^{-1}$ region of the IR spectrum that can be attributed to the stretching modes of the NO_3 group [122,123]. These bands are consistent with those previously reported for analogous silver(I) phosphane complexes [124–126]. However, the multiplicity of the observed bands prevents an unambiguous assignment of the nitrate group's coordination mode—whether monodentate or bidentate—to the metal center.

The ^1H -NMR spectra of **4**, **8**, and **9** in DMSO-d_6 showed a set of resonances in agreement with the proposed structure. The slightly shifted resonance at δ 15.45–16.38 ppm corresponds to the OH phenolic proton. In the spectra **4** and **9**, the NCH_2P protons of PTA co-ligands are visible as singlets at δ 4.15–4.16 ppm and the related NCH_2N protons show characteristic AB quartets in the range of 4.40–4.58 ppm. In the spectrum of complex **8**, the aromatic hydrogens of the ligand and triphenylphosphine co-ligands are detectable in the range 6.71–7.63 ppm. In the ^{31}P -NMR spectra of the PTA complexes **4** and **9** recorded in CDCl_3 , a singlet is visible at $-\text{93.60}$ and $-\text{94.43}$ ppm, downfield shifted with respect to the value of the free PTA (δ $-\text{102.50}$ ppm). Broad signals are also in the spectra recorded in CD_3OD and CD_3CN at 233K, indicating the impossibility to stop or slow the phosphane exchange process, to show doublets in which the coupling of ^{31}P to the ^{107}Ag and ^{109}Ag are resolved. In the ^{31}P -NMR spectrum of the triphenylphosphine complex **8** recorded in CDCl_3 at room temperature, a very broad singlet is visible at 14.68 ppm, downfield shifted with respect to the value of the free PPh_3 (δ $-\text{5.34}$ ppm). In the spectrum of

8 recorded in CD₃CN at 233K, a doublet was observed. The related $J(\text{Ag}-^{31}\text{P})$ coupling constant (478 Hz) is of the same order of magnitude of those reported for analogous silver(I) bis(triphenylphosphine) species [111,127–130]. ^1H -NMR and $^{31}\text{P}\{^1\text{H}\}$ -NMR data of complexes **4**, **8**, and **9** are summarized in Table S1. The ESI-MS study was performed by dissolving complexes **4**, **8**, and **9** in methanol or acetonitrile and recording the spectra in ion-positive and ion-negative modes. In the ESI-MS(+) spectrum of **4** and **9**, the peaks at m/z 491 and 553 can be attributed to the species $[\text{Ag}(\text{HL}^{\text{BSMe}})(\text{PTA})]^+$ and $[\text{Ag}(\text{HL}^{\text{BSPH}})(\text{PTA})]^+$, respectively, confirming the formation and the stability of the complexes.

2.2. X-Ray Crystallography

Despite several efforts, we were able to get crystalline samples of only one of the aforementioned compounds. In particular, the structure of the $[\text{Cu}(\text{L}^{\text{BSPH}})_2]$ complex (**10**) was determined by single-crystal diffraction analysis on an item extracted from a batch of very good, dark green prismatic specimens, obtained by a slow recrystallization of the compound from a toluene solution. The investigation revealed that the neutral complex crystallizes in the monoclinic system; the solid-state structure was solved in the centrosymmetric $I2/a$ space group (No. 15). The asymmetric unit (Figure 1) consists of one half of the molecule, that is, the copper ion, and a single molecule of the anionic 2-(benzylimino(phenyl)methyl)phenolate (L^{BSPH}) ligand, which chelates the central Cu atom through the O, N atoms. The phenyl ring of the benzylimino residue of the ligand (C15/C20) is disordered over two possible arrangements; the alternate positions of disordered atoms have been named with a final 'A'.

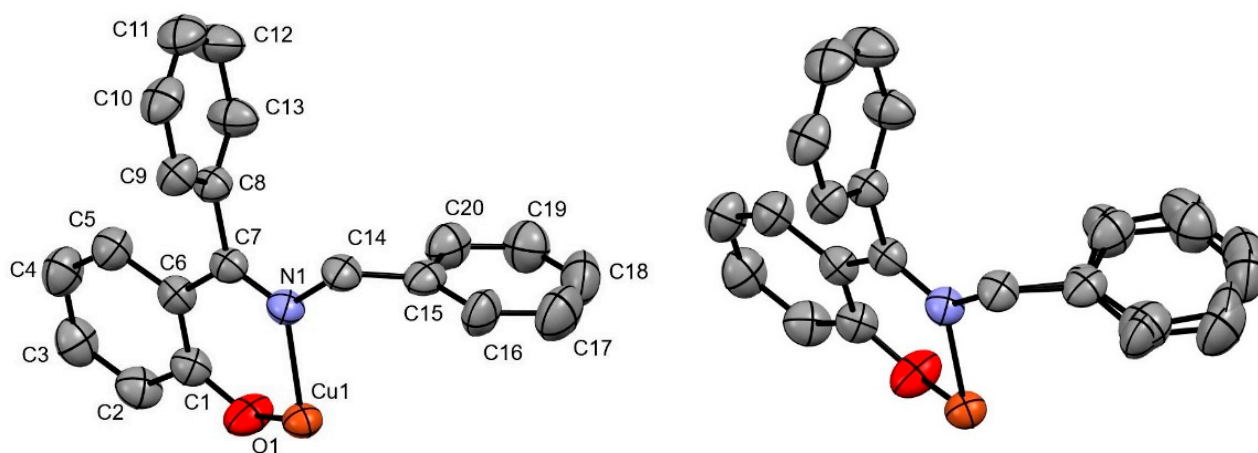


Figure 1. (Left): a drawing of the asymmetric unit of $[\text{Cu}(\text{L}^{\text{BSPH}})_2]$ (**10**), showing the numbering scheme; disorder not shown. (Right): same view highlighting the disorder of the phenyl ring C15/C20. Hydrogen atoms omitted; thermal ellipsoids at 50% probability.

Upon chelation, the ligand and the metal form a six-membered metallacycle (Cu1, O1, C1, C6, C7, N1), showing an *envelope* conformation, with the Cu1 atom ‘at the flap’ and departing by 0.55 Å from the mean plane (p1) of the other five atoms, that are instead coplanar within 0.05 Å, given the sp^2 nature of the C6–C7–N1 atoms of the ligand. In the chelating L^{BSPH} molecule, the mean plane of the phenol ring (C1/C6) is almost coplanar with p1 (angle of 1.39°); instead, the mean planes passing through the phenyl rings of the benzyl moiety (C15/C20 or C15A/C20A, respectively, p2 and p2') or emerging from the methine bridge (C8/C13, p3) are approximately orthogonal to the p1 plane, making with the latter angles of 79.1° (79.6° for p2'), and 75.2°, respectively. The p3 and p2 planes are also roughly orthogonal with respect to each other (angles of 69.9° and 72.2° for p2 and p2', respectively).

The copper coordination environment is completed by a second L^{BSPH} molecule (Figure 2), in which both the O1 and N1 atoms are *trans*-positioned to their symmetry-generated counterparts. The $[Cu(L^{BSPH})_2]$ complex (**10**) has a calix shape when observed through the O_2N_2 coordination plane and the four coordinating atoms around the central copper atom define a moderately distorted square planar environment (τ_4 and τ_4' indexes of 0.21 and 0.18, respectively) [131,132], with O1-Cu1-O1* and N1-Cu1-N1* (* = $3/2 - x, y, 1 - z$) angles of $160.77(9)^\circ$ and $170.07(7)^\circ$, respectively—the first quite far from the ideal 180° value. Apparently, the departure is due to the engagement of the O1 atom in an intermolecular non-canonical hydrogen bond with the H18 atom of a nearby phenyl ring (see further below).

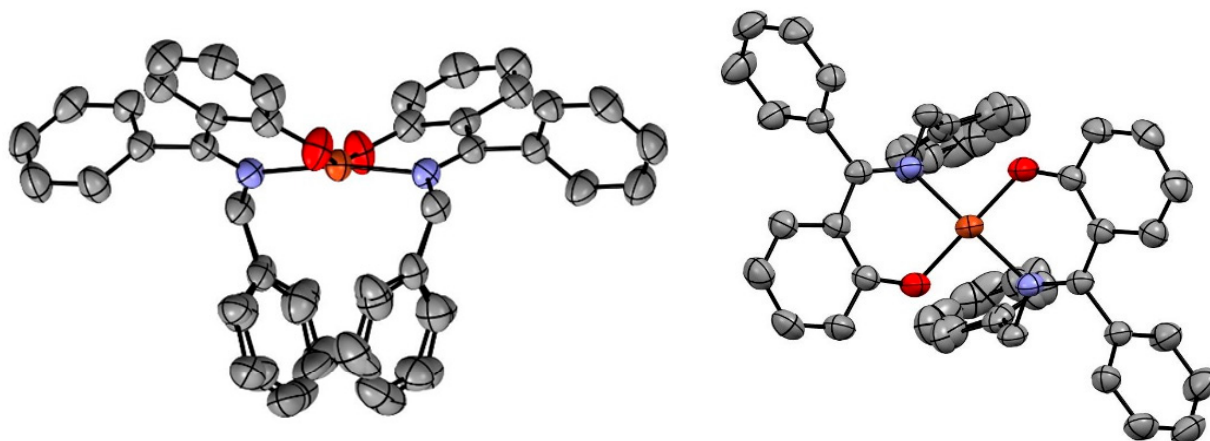


Figure 2. Two orthogonal views of the $[Cu(L^{BSPH})_2]$ complex. (Left): overall view of the complex looking through the coordination plane, highlighting its calix shape; (right): view of the Cu(II) coordination plane. Hydrogen atoms omitted; thermal ellipsoids at 50% probability.

With respect to bond distances and angles, the 2-(benzylimino(phenyl)methyl)phenolate ligand does not show unusual metric values when compared to existing data. An investigation in the CCDC database [133] for molecules showing the benzyl(diphenylmethylene)amine moiety returned about 50 entries. A comparison of bond distances next to the C=N link with those found in this work showed that the object with the best overall similarity, that is, with the smaller sum of deviations for examined distances, is the (already reported) ligand itself [121], besides few other compounds [134,135]. Interestingly, molecules in which the C=N distance is close to the one reported here ($1.299(2) \text{ \AA}$) are those in which a phenolic moiety was also present [121,136–138]. The C=N bond participates in some degree of conjugation with the nearby phenyl rings, in known compounds as well as in the present complex. In fact, the C6-C7 and C7-C8 bonds are a little shorter than the ideal 1.54 \AA ($1.4654(19)$ and $1.5009(19) \text{ \AA}$, compared with mean values of 1.494 and 1.492 \AA for known molecules); the same is true for the N1-C14, C14-C15 distances in the benzyl residue ($1.4787(17)$, $1.483(10) \text{ \AA}$ against corresponding mean values of 1.450 and 1.517 \AA in reported compounds). These data suggest that bond conjugation in the ligand is little affected by coordination.

A second search in the CCDC repository was made to seek transition metal complexes showing a ligand similar to L^{BSPH} . The search returned a very limited number of Mn, Co, Ni, and Cu compounds showing a tetradentate dimeric form of the L^{BSPH} ligand, all prepared by the same research group [139–143]; to the best of our knowledge, then, **10** is the first Cu(II) complex of the L^{BSPH} ligand reported to date. In known molecules, the O and N donor atoms are always *trans* to each other, opposite to what happens in the $[Cu(L^{BSPH})_2]$ complex. The Metal-O, Metal-N distances in these molecules fall in the ranges 1.82 – 1.91 \AA , 1.85 – 2.03 \AA , respectively, with differences basically due to the ionic radii of the elements. In fact, the mean values for the Cu-O, Cu-N distances in the Cu(II) known complexes [140]

(1.879 and 1.949 Å, respectively) are in very good/good agreement with the 1.8839(11) and 1.9773(12) Å found here. A complete listing of bond lengths and angles for complex **10** is provided in the supporting information (Tables S2 and S3).

The examination of relevant nonbonding interactions (metric details listed in Table 1), mostly hydrophobic contacts, shows that the complex units are well packed, and that the unit cell does not show solvent accessible voids. Looking at the asymmetric unit (one half of the complex), just one intermolecular hydrogen bond connects H18 (or H18A) with the O1 atom of a nearby molecule at $3/2 - x, -1 + y, 1 - z$ (at 2.81/2.85 Å, respectively); this interaction also shows in the symmetry-generated half of the molecule at $1/2 - x, y, 1 - z$ (Figure 3; further packing diagrams highlighting the other contacts described here can be found in Figures S34–S36 of supporting information). Incidentally, the two symmetry-related halves of the complex have their C15/C20 (or C15A/C20A) rings in roughly eclipsed positions, so they are also coupled by somehow weak $\pi \cdots \pi$ interactions, with distances between planes encompassing the alternate arrangements of the rings of 4.20, 4.03 Å, respectively, (compared with 3.35 Å in graphite).

Table 1. Relevant nonbonding interactions for $[\text{Cu}(\text{L}^{\text{BSPH}})_2]$ (**10**).

A Atom	D Atom	P Atom ^a	A...D (Å)	A...D–P (°)	Symmetry Op. ^b
O1	H18	C18	2.81	171.8	$3/2 - x, y, 1 - z$
O1	H18A	C18	2.85	159.9	$3/2 - x, y, 1 - z$
C15/C20	H11	C11 ^c	2.78 ^d	168.8 ^d	$1 - x, -1/2 + y, 1/2 - z$
C15A/C20A	H11	C11 ^c	2.78 ^d	165.0 ^d	$1 - x, -1/2 + y, 1/2 - z$
C1	H12	C12 ^c	2.91	147.7	$1 - x, 1 - y, 1 - z$
C2	H12	C12 ^c	2.91	145.7	$1 - x, 1 - y, 1 - z$
C15/C20	C15/C20 ^e		4.20 ^f	26.6 ^g	$1/2 - x, y, 1 - z$
C15A/C20A	C15A/C20A ^e		4.03 ^f	23.4 ^g	$1/2 - x, y, 1 - z$

^a Atom to which D atom is bound; ^b symmetry operations related to asymmetric unit = x, y, z ; ^c C–H... π interactions; ^d distances and angles referring to selected ring centroids; ^e $\pi \cdots \pi$ interactions; ^f distance between ring centroids; ^g angle between mean planes encompassing phenyl rings.

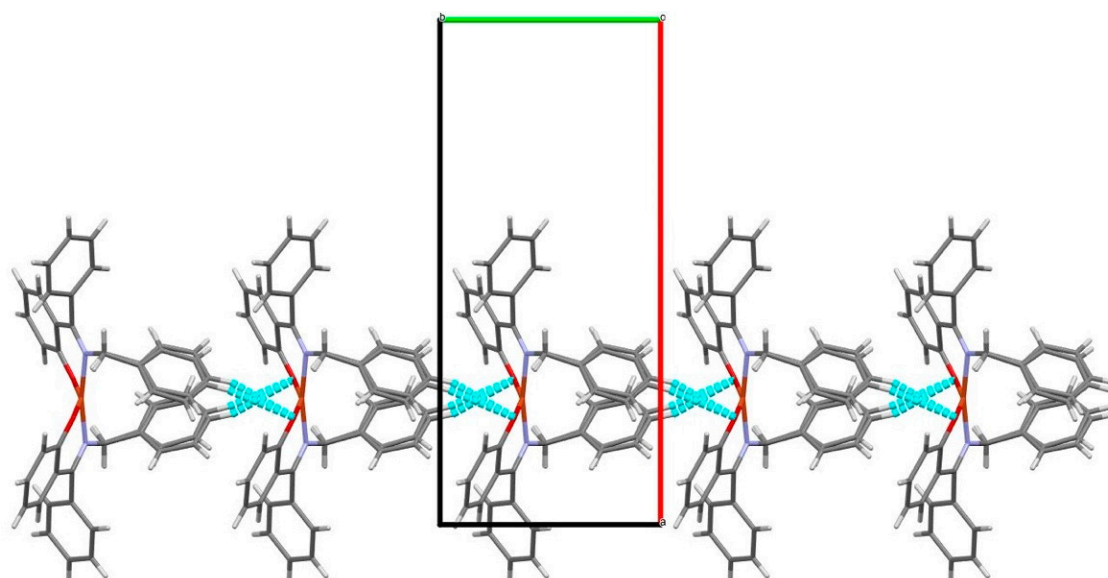


Figure 3. Nonbonding contacts for $[\text{Cu}(\text{L}^{\text{BSPH}})_2]$; projection down the crystallographic c axis, highlighting the one-dimensional motif generated by the $\text{O1} \cdots \text{H18}$, $\text{O1} \cdots \text{H18A}$ hydrogen bonds (in cyan) and propagating along the crystallographic b axis. The $\pi \cdots \pi$ pairing of the C15/C20, C15A/C20A rings with the corresponding symmetry-generated counterparts is also visible. Other contacts omitted for clarity.

The H18...O1 contact creates a one-dimensional motif which propagates along the crystallographic b axis, and it is coupled to a second orthogonal chain due to the C-H... π contacts made by C1/C2 atoms and the H12 atom of another unit at $1 - x, 1 - y, 1 - z$ (Figure S36). The two chains cross-link each other and create a 2D grid in the ab plane (Figure S37). Finally, a third chain is formed by a second, T-shaped C-H... π contact involving the C15/C20 (or C15A/C20A) ring with the H11 atom of a nearby molecule at $1 - x, -1/2 + y, 1/2 - z$ (Figure S38; only C15...H11 approach shown). The H11 atom in fact points almost straight towards the C15/C20 ring centroid, with a contact length of 2.78 Å (also towards the C15A/C20A ring) and C11-H11-ring centroid angle of 168.8° and 165.0° for C15/C20, C15A/C20A rings, respectively. This chain propagates along the [011] plane and diagonally intersects the above described 2D motif, thus sealing a full 3D contact network.

2.3. In-Vitro Antibacterial Activity

First, the resazurin-based microtiter dilution assay (RMDA) method was used to evaluate the synergic antibacterial effect of Schiff bases (**1** and **2**), metal complexes (**3–10**), and phosphane co-ligands (**11** and **12**). Figures 4 and 5 show the bacterial growth curves against Gram-negative (*E. coli*) and Gram-positive bacteria (*S. aureus*), respectively. The minimum inhibitory concentrations (MIC) were reported in Table 2 and half-maximal inhibitory concentrations (MIC₅₀) values were calculated using computerized nonlinear regression analysis.

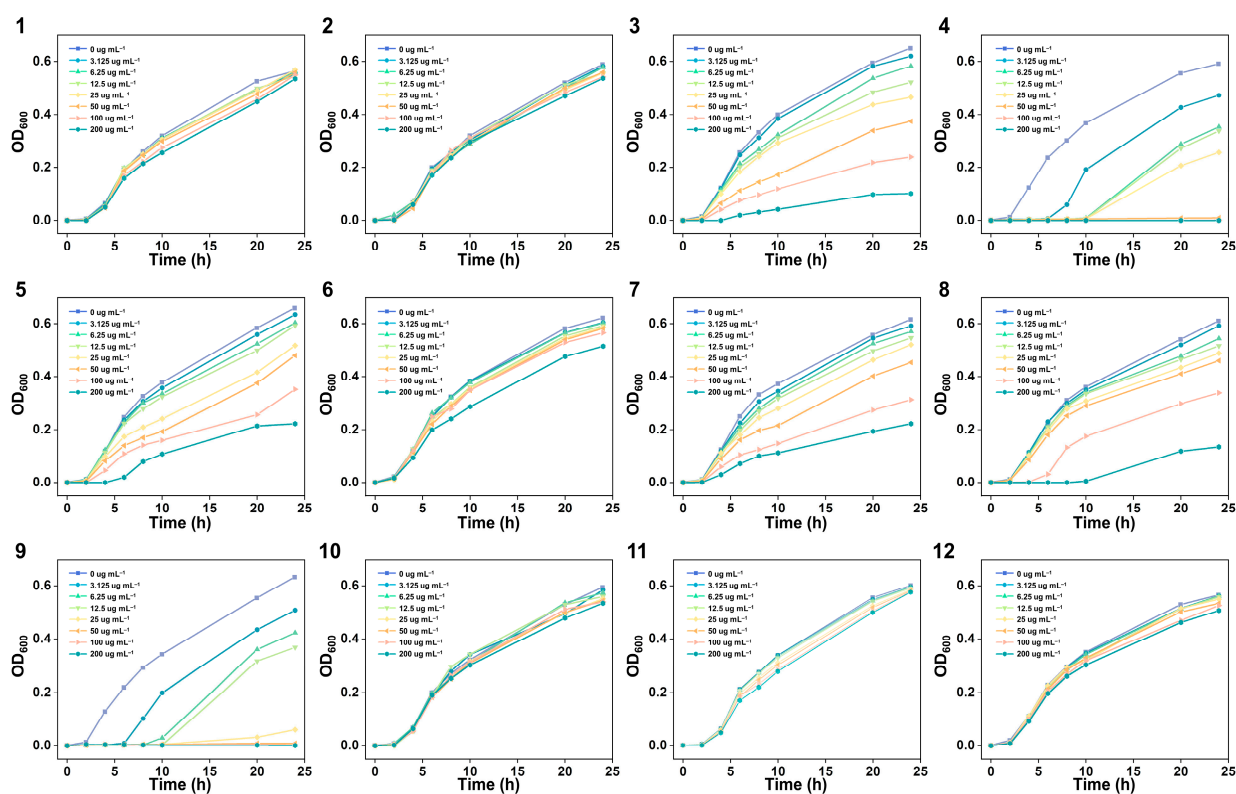


Figure 4. Bacterial growth curves of *E. coli* after treatment with Schiff base ligands (**1** and **2**), metal complexes (**3–10**), and phosphane co-ligands (**11** and **12**).

Generally, the growth of bacteria follows four phases: lag phase, logarithmic phase, stationary phase, and decline phase. When bacteria are exposed to external interferences or inhibitory factors, their growth may be significantly delayed or even completely suppressed, ultimately leading to growth cessation.

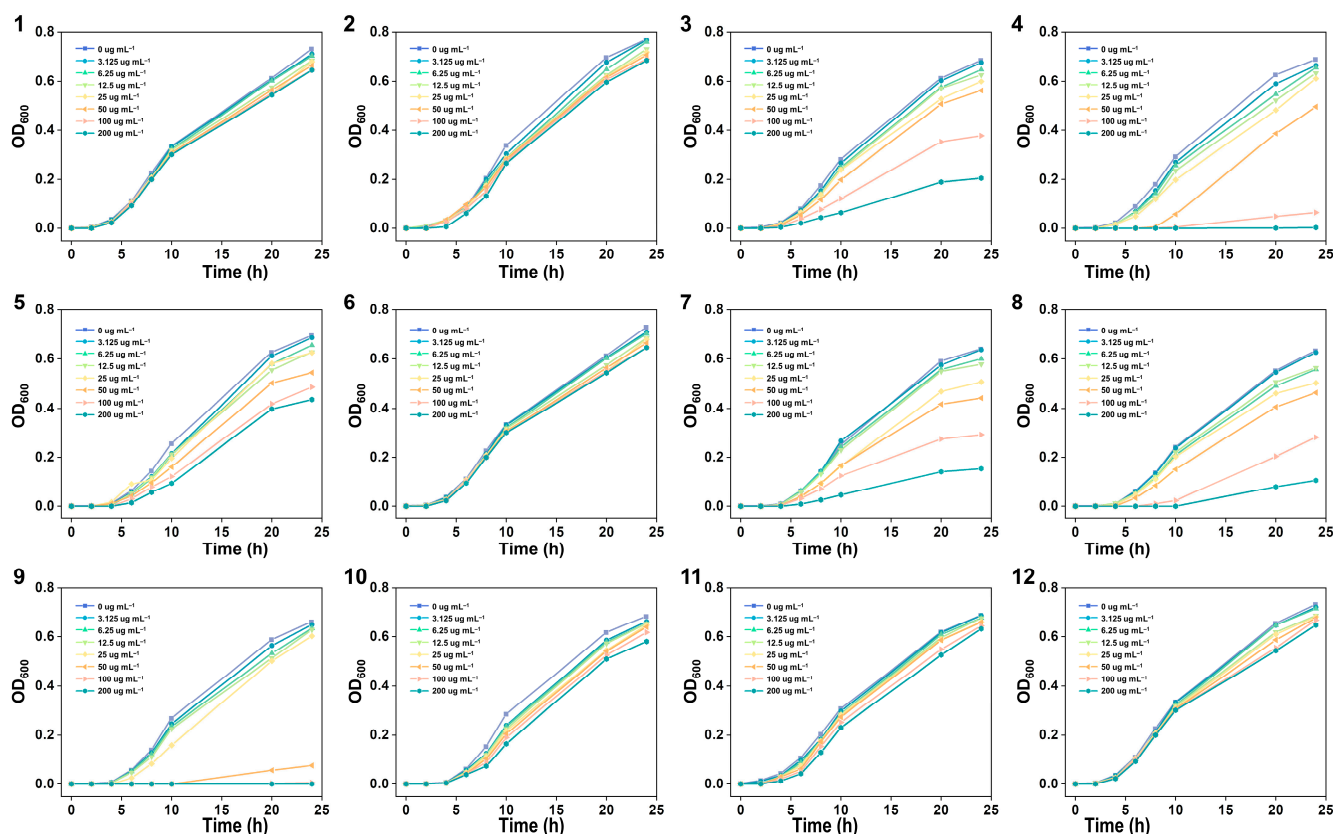


Figure 5. Bacterial growth curves of *S. aureus* after treatment with Schiff base ligands (**1** and **2**), metal complexes (**3–10**), and phosphane co-ligands (**11** and **12**).

Table 2. MIC and MIC₅₀ values of Schiff base ligands (**1** and **2**), metal complexes (**3–10**), and co-ligands (**11** and **12**) in-vitro antimicrobial screening.

N.	Tested Compounds	<i>E. coli</i>		<i>S. aureus</i>	
		MIC	MIC ₅₀	MIC	MIC ₅₀
1	HL ^{BSMe}	/	/	/	/
2	HL ^{BSPH}	/	/	/	/
3	[Cu(HL ^{BSMe})(PTA) ₂] ₂ PF ₆	/	0.057 (0.076)	/	0.116 (0.149)
4	[Ag(HL ^{BSMe})(PTA)]NO ₃	0.050 (0.090)	0.012 (0.021)	0.100 (0.181)	0.061 (0.110)
5	[Cu(L ^{BSMe}) ₂]	/	0.110 (0.210)	/	0.381 (0.738)
6	[Cu(HL ^{BSPH})(PPh ₃) ₂] ₂ PF ₆ ·2CH ₃ CN	/	/	/	/
7	[Cu(HL ^{BSPH})(PTA) ₂] ₂ PF ₆ ·2H ₂ O	/	0.114 (0.130)	/	0.084 (0.100)
8	[Ag(HL ^{BSPH})(PPh ₃) ₂] ₂ NO ₃	/	0.098 (0.100)	/	0.080 (0.079)
9	[Ag(HL ^{BSPH})(PTA)]NO ₃	0.025 (0.040)	0.010 (0.016)	0.050 (0.081)	0.036 (0.058)
10	[Cu(L ^{BSPH}) ₂]	/	/	/	/
11	PPh ₃	/	/	/	/
12	PTA	/	/	/	/

MIC and MIC₅₀ calculated in mg mL^{−1} (mM in parentheses); “/”: more than 0.381 mg mL^{−1} and 0.738 mM.

Based on the bactericidal growth curves, the free Schiff base ligands and phosphane co-ligands exhibited negligible toxicity against both Gram-negative and Gram-positive bacterial species, while all the metal complexes demonstrated different antibacterial activities. Especially, the silver complexes [Ag(HL^{BSMe})(PTA)]NO₃ (**4**) and [Ag(HL^{BSPH})(PTA)]NO₃ (**9**) showed a significant bactericidal effect. The MIC values of compound **4** against *E. coli* and *S. aureus* were 0.050 and 0.100 mg mL^{−1}, respectively, while the MIC values of compound **9** were 0.025 and 0.050 mg mL^{−1}, respectively. Interestingly, the MIC values of

compound **4** were higher in comparison to the values of **9**; however, the bacterial growth curves indicated that the growth rate of bacteria treated with compound **4** was slower when the concentrations were below 0.025 mg mL^{-1} . Their different bacterial growth behaviors can lie in the structure of the Schiff base ligands with the presence of a methyl or a phenyl substituent in compounds **4** and **9**, respectively. Previous studies have suggested that the bactericidal activity of silver compounds is primarily due to two distinct mechanisms, including the strong affinity to R-SH groups associated in amino acids or proteins and their ability to generate reactive oxygen species (ROS). Silver ions can readily bind to SH groups, such as those in cysteine residues, which can disrupt cellular metabolism and physiology by directly interfering with enzymatic functions or by destabilizing disulfide (S-S) bonds critical for maintaining protein structure. However, effective binding to SH groups requires silver ions to be sufficiently accessible and reactive [144,145].

The bactericidal activities of the compounds at different concentrations were further evaluated using the plate colony count method against *E. coli* (Figure 6) and *S. aureus* (Figure 7). The minimum bactericidal concentration (MBC) and half-maximal bactericidal concentration (MBC_{50}) were calculated and included in Table 3.

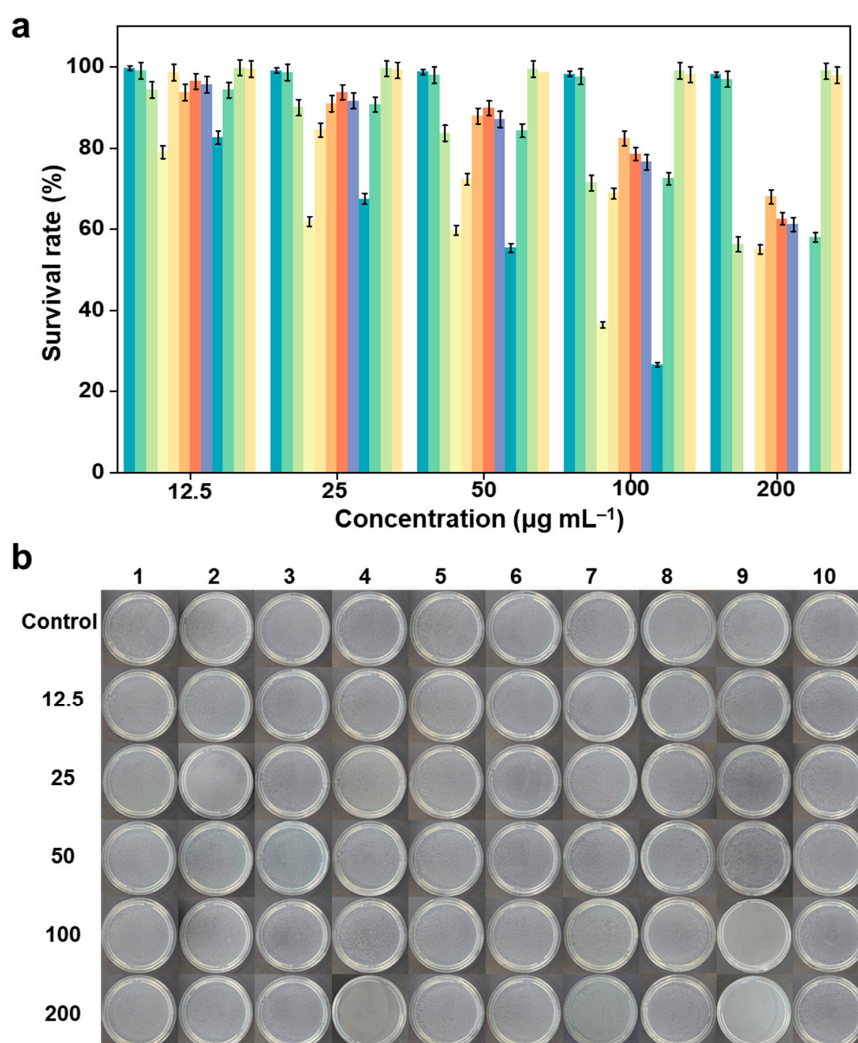


Figure 6. (a) The bacterial viability of compounds **1–12** (from left to right) with different concentration and (b) corresponding bacterial colony images of *E. coli*. Colonies were quantified with ImageJ software (1.50d) and presented as mean values from duplicate independent experiments. Error bars denote standard deviation. The significance level between the control and treated samples was established at $p < 0.05$.

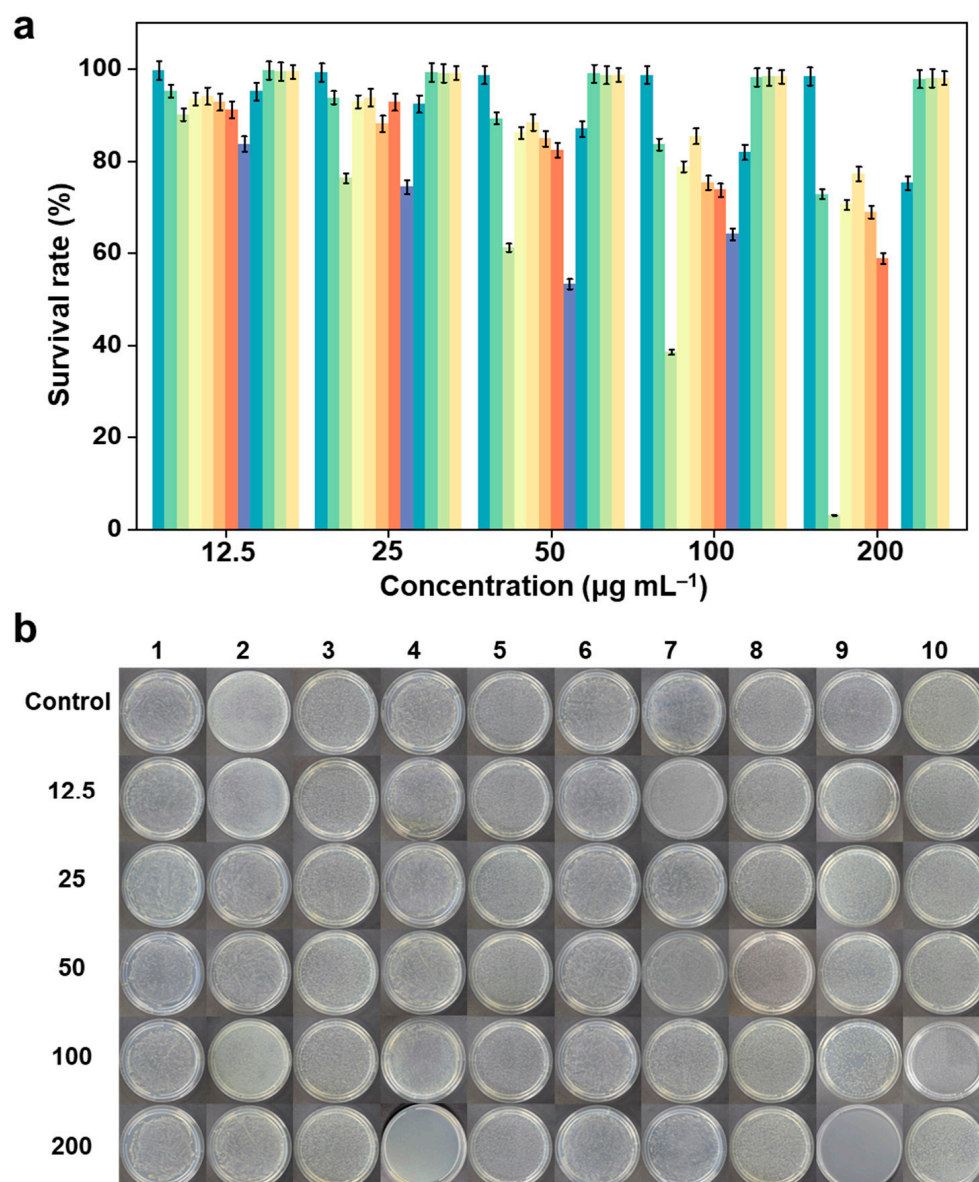


Figure 7. (a) The bacterial viability of compounds 1–12 (from left to right) with different concentrations and (b) corresponding bacterial colony images of *S. aureus*. Colonies were quantified with ImageJ software (1.50d) and presented as mean values from duplicate independent experiments. Error bars denote standard deviation. The significance level between the control and treated samples was established at $p < 0.05$.

The results demonstrate that the antimicrobial activities of the metal complexes 3–9 are significantly enhanced compared to the free Schiff base ligands, which can be explained by Tweedy’s chelation theory. Due to the electron donating properties of Schiff base ligands, a metal ion can share part of its charge through orbital overlap with Schiff base ligands, which reduces the polarity of the metal ion. Furthermore, this process increases the lipophilicity of the central metal atom, facilitating its penetration through the lipid layer of the microorganism, and blocking the interaction of enzymes on the cell membrane, thereby inhibiting the growth of the microorganism [146,147]. Subsequently, Cu(I) and Ag(I) coordination compounds were investigated to study the influence of the nature of a metal center in bioactivity. A comparison of the antimicrobial properties of compounds 3 and 4, 6 and 8, as well as 7 and 9 reveals that silver complexes exhibit superior antimicrobial effects against both *E. coli* and *S. aureus* strains compared to their copper-based counterparts.

Among these metal complexes, compound **9** was found to be most active against the bacterial strains with MBC values of 0.100 and 0.200 mg mL^{−1} for *E. coli* and *S. aureus*, respectively. Additionally, compound **4** was prominently active with MBC values of 0.200 mg mL^{−1} against both tested bacterial strains. Compound **8** displayed moderate inhibitory effects with MBC₅₀ values of 0.322 and 0.294 mg mL^{−1}, however lower than the MBC₅₀ values of 0.566 and 1.125 mg mL^{−1} for compound **6**. As previously mentioned, Ag(I) ions have the ability to alter the bacteria cell wall structure and cell constituent by irreversibly binding to cysteine residues, thereby disrupting essential enzyme systems and ultimately inhibiting bacterial proliferation [144,148].

Table 3. MBC and MBC₅₀ values of Schiff base ligands (**1** and **2**), metal complexes (**3–10**), and co-ligands (**11** and **12**) in-vitro antimicrobial screening.

N.	Tested Compounds	<i>E. coli</i>		<i>S. aureus</i>	
		MBC	MBC ₅₀	MBC	MBC ₅₀
1	HL ^{BSMe}	/	/	/	/
2	HL ^{BSPH}	/	/	/	/
3	[Cu(HL ^{BSMe})(PTA) ₂ PF ₆	/	0.262 (0.350)	/	0.642 (0.858)
4	[Ag(HL ^{BSMe})(PTA)]NO ₃	0.200 (0.362)	0.048 (0.086)	0.200 (0.362)	0.062 (0.112)
5	[Cu(L ^{BSMe}) ₂]	/	0.243 (0.474)	/	0.578 (1.128)
6	[Cu(HL ^{BSPH})(PPh ₃) ₂]PF ₆ ·2CH ₃ CN	/	0.566 (0.513)	/	1.125 (1.020)
7	[Cu(HL ^{BSPH})(PTA) ₂]PF ₆ ·2H ₂ O	/	0.319 (0.377)	/	0.551 (0.651)
8	[Ag(HL ^{BSPH})(PPh ₃) ₂]NO ₃	/	0.322 (0.327)	/	0.294 (0.299)
9	[Ag(HL ^{BSPH})(PTA)]NO ₃	0.100 (0.163)	0.046 (0.075)	0.200 (0.326)	0.068 (0.110)
10	[Cu(L ^{BSPH}) ₂]	/	0.282 (0.443)	/	0.875 (1.375)
11	PPh ₃	/	/	/	/
12	PTA	/	/	/	/

MBC and MBC₅₀ calculated in mg mL^{−1} (mM in parentheses); “/”: more than 1.125 mg mL^{−1} and 1.375 mM.

Furthermore, a possible correlation between the biological activity of the compounds and their lipophilicity and hydrophilicity was discussed. By comparing compounds **6** and **7**, as well as **8** and **9**, it was observed that the antibacterial activity of the complexes with PTA as a co-ligand was superior to those with PPh₃ as a co-ligand. Notably, the lipophilic triphenylphosphine and the hydrophilic 1,3,5-triaza-7-phosphaadamantane have been chosen as co-ligands because they can stabilize copper and silver in +1 oxidation state and can give also a different hydrophilic–lipophilic balance to the corresponding complexes. The antibacterial data indicate that the PTA co-ligands confer the related silver complexes the most appropriate balance between hydrophilicity and lipophilicity [149–152], what is in fact a major challenge in the development of antimicrobial agents. The presence of lipophilic groups enhances penetration ability to the bacterial lipophilic outer membrane which contains murein, thereby facilitating interactions with the bacterial replicative system [144,145]. However, several studies have also highlighted the importance of water solubility as a key parameter in antibacterial activity.

The antibacterial performance of the synthesized compounds was systematically evaluated with respect to three critical determinants: (i) ligands chelation effects on bioavailability, (ii) properties of metal ions, and (iii) hydrophobic–lipophilic balance. Compared to the broad-spectrum antibiotic ciprofloxacin (Figure 8), although the synthesized metal complexes are less effective than the standard drug, compounds **4** and **9** have demonstrated significant potential as antibacterial agents. In addition, compared with other silver Schiff base metal complexes reported for antibacterial applications, the compounds **4** and **9** exhibits similar or lower MIC values [65,66,85,144,153–156].

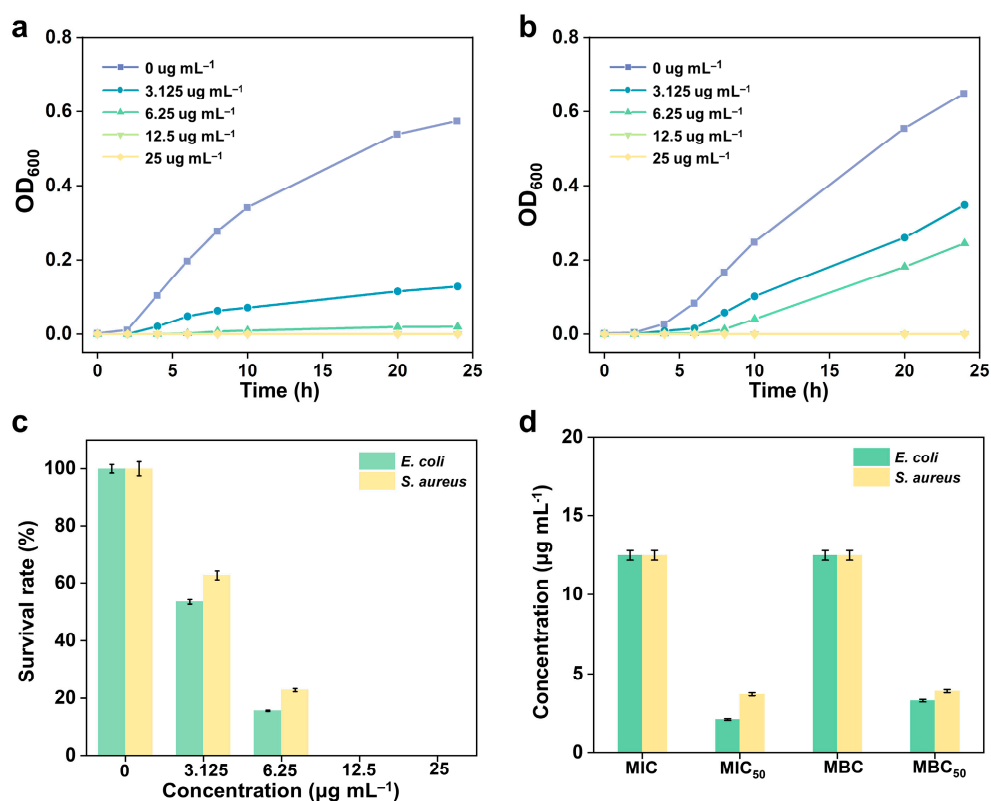


Figure 8. Bacterial growth curves of (a) *E. coli* and (b) *S. aureus* after treatment with ciprofloxacin. (c) Corresponding bacterial viability of *E. coli* (green) and *S. aureus* (yellow) after treatment with ciprofloxacin. (d) The summary of antimicrobial activity of ciprofloxacin.

3. Experimental Section

3.1. Materials and Instruments

All reagents were obtained from commercial suppliers and used as received. Melting Points (MP) were performed by an SMP3 Stuart Scientific Instrument (Bibby Sterilin Ltd., London, UK). Elemental analyses (C, H, N, S) (EA) were performed with a Fisons Instruments EA-1108 CHNS-O Elemental Analyzer (Thermo Fisher Scientific Inc., Waltham, MA, USA). Fourier-Transform InfraRed (FT-IR) spectra were recorded from 4000 to 700 cm^{-1} on a PerkinElmer Frontier Instrument (PerkinElmer Inc., Waltham, MA, USA), equipped with an Attenuated Total Reflection (ATR) unit using universal diamond top-plate as a sample holder. Abbreviations used in the analyses of the FT-IR spectra: br = broad, m = medium, mbr = medium broad, s = strong, sbr = strong broad, vs. = very strong, w = weak, wbr = weak broad. Nuclear Magnetic Resonance (NMR) spectra for the nuclei ^1H , ^{13}C and ^{31}P were recorded with a Bruker 500 Ascend Spectrometer (Bruker BioSpin Corporation, Billerica, MA, USA; 500.13 MHz for ^1H , 125.78 MHz for ^{13}C , 202.46 MHz for ^{31}P and 470.59 MHz for ^{19}F). Tetramethylsilane (SiMe_4) was used as external standard for the ^1H - and ^{13}C -NMR spectra, while 85% H_3PO_4 was used for the ^{31}P -NMR spectra. The chemical shifts (δ) are reported in ppm, and coupling constants (J) are reported in hertz (Hz). Abbreviations used in the analyses of the NMR spectra: br = broad, d = doublet, dbr = broad doublet, m = multiplet, s = singlet, sbr = broad singlet, t = triplet. ElectroSpray Ionization Mass Spectra (ESI-MS) were recorded in positive- (ESI-MS(+)) or negative-ions (ESI-MS(−)) mode on a Waters Micromass ZQ Spectrometer equipped with a single quadrupole (Waters Corporation, Milford, MA, USA), using methanol or an acetonitrile mobile phase. The compounds were added to reagent grade methanol or acetonitrile to give approximately 0.1 mM solutions. These solutions were injected (1 μL) into the spectrometer fitted with

an autosampler. The pump delivered the solutions to the mass spectrometer source at a flow rate of 200 $\mu\text{L}/\text{min}$ and nitrogen was employed both as a drying and nebulizing gas. The capillary voltage was typically 2500 V. The temperature of the source was 100 $^{\circ}\text{C}$, while the temperature of the desolvation was 400 $^{\circ}\text{C}$. In the analyses of ESI-MS spectra, the confirmation of major peaks was supported by comparison of the observed and predicted isotope distribution patterns, the latter calculated using the IsoPro 3.1 computer software (T-Tech Inc., Norcross, GA, USA).

3.2. Synthesis

3.2.1. Synthesis of the Ligand HL^{BSMe} (1)

The ligand (*E*)-2-(1-(benzylimino)ethyl)phenol, HL^{BSMe} (1) was prepared by the reaction of 1-(2-hydroxyphenyl)ethan-1-one (1.100 mmol, 0.150 g) and benzylamine (1.000 mmol, 0.107 g) in methanol (30 mL). The mixture was stirred at room temperature for 4 h, monitored via TLC, until the complete consumption of acylphenol. The mixture was evaporated at reduced pressure and dissolved in CH_2Cl_2 (25 mL) and 1M solution of NaOH (4×8 mL). After extraction, the organic phase was anhydriified with Na_2SO_4 , evaporated and dried at reduced pressure, giving the product HL^{BSMe} in 80% yield. Solubility: CH_3OH , $\text{CH}_3\text{CH}_2\text{OH}$, CH_3CN , CHCl_3 , Acetone, EtOAc, DMSO. M.p.: 118–119 $^{\circ}\text{C}$. FT-IR (cm^{-1}): 3211wbr, 3108vw, 3061w, 3034w, 2918w, 2877w, 2814w (C-H); 1610s, 1572m (C=C and C=N); 1492m, 1451s, 1413m, 1376m, 1350m, 1330m, 1303s, 1263m, 1232m, 1181w, 1161m, 1129m, 1074w, 1055m, 1024m, 974m, 950m, 941m, 928m, 900m, 860m, 831m, 743vs, 733vs, 698vs, 639m, 584m, 559m, 525m, 501m. ^1H -NMR (CDCl_3 , 293K): δ 2.51 (s, 3H, CH_3), 4.87 (s, 2H, CH_2), 6.83–7.61 (m, 9H, CH_{ar}), 15.78 (sbr, 1H, OH). ^1H -NMR (CD_3CN , 293K): δ 2.48 (s, 3H, CH_3), 4.83 (s, 2H, CH_2), 6.83–7.71 (m, 9H, CH_{ar}), 16.23 (sbr, 1H, OH). ^1H -NMR (Acetone- d_6 , 293K): δ 2.52 (s, 3H, CH_3), 4.88 (s, 2H, CH_2), 6.80–7.72 (m, 9H, CH_{ar}), 15.87 (sbr, 1H, OH). ^1H -NMR (DMSO- d_6 , 293K): δ 2.51 (s, 3H, CH_3), 4.83 (s, 2H, CH_2), 6.78–7.72 (m, 9H, CH_{ar}), 16.37 (sbr, 1H, OH). $^{13}\text{C}\{^1\text{H}\}$ -NMR (CDCl_3 , 293K): δ 14.7 (CH_3), 53.4 (CH_2), 117.2, 118.8, 119.5, 127.2, 127.5, 128.1, 128.8, 132.6, 138.5 (CH_{Ar}), 163.8 (COH), 172.2 (C=N). ESI-MS(+) (major positive ions, CH_3CN), m/z (%): 226 (100) [$\text{L}^{\text{BSMe}} + \text{H}$] $^+$. Elemental analysis (%) calculated for $\text{C}_{15}\text{H}_{15}\text{NO}$: C 79.97, H 6.71, N 6.22; found: C 80.25, H 6.54, N 6.36.

3.2.2. Synthesis of the Ligand HL^{BSPH} (2)

The ligand (*E*)-2-((benzylimino)(phenyl)methyl)phenol, HL^{BSPH} (2) was prepared following the procedure described for ligand 1, using (2-hydroxyphenyl)(phenyl)methanone (1.100 mmol, 0.218 g) and was obtained in 72% yield. Solubility: CH_3OH , $\text{CH}_3\text{CH}_2\text{OH}$, CH_3CN , CHCl_3 , Acetone, EtOAc, DMSO. M.p.: 89–91 $^{\circ}\text{C}$. FT-IR (cm^{-1}): 30,653w, 3026w, 2988w, 2966w, 2922w, 2858w (C-H); 1604s, 1563m (C=C and C=N); 1498m, 1446m, 1378m, 1355w, 1350w, 1299m, 1266m, 1227m, 1203m, 1165m, 1153m, 1126m, 1094m, 1075m, 1049m, 1028m, 993m, 948m, 912m, 856w, 829m, 798m, 752vs, 711m, 697s, 676m, 627m, 588m. ^1H -NMR (CDCl_3 , 293K): δ 4.59 (s, 2H, CH_2), 6.68–7.56 (m, 14H, CH_{ar}), 15.64 (sbr, 1H, OH). ^1H -NMR (CD_3CN , 293K): δ 4.55 (s, 2H, CH_2), 6.70–7.60 (m, 14H, CH_{ar}), 15.42 (sbr, 1H, OH). $^{13}\text{C}\{^1\text{H}\}$ -NMR (CD_3CN , 293K): δ 55.3 (CH_2), 117.5, 117.6, 120.0, 127.1, 127.4, 127.6, 128.6, 128.8, 129.2, 131.6, 132.5, 133.9, 139.4 (CH_{Ar}), 162.9 (COH), 174.8 (C=N). ESI-MS(+) (major positive ions, CH_3CN), m/z (%): 288 (100) [$\text{L}^{\text{BSPH}} + \text{H}$] $^+$. Elemental analysis (%) calculated for $\text{C}_{20}\text{H}_{17}\text{NO}$: C 83.59, H 5.96, N 4.87; found: C 83.42, H 5.73, N 4.92.

3.2.3. Synthesis of $[\text{Cu}(\text{HL}^{\text{BSMe}})(\text{PTA})_2]\text{PF}_6$ (3)

Tetrakis(acetonitrile)copper(I)hexafluorophosphate (0.500 mmol, 0.186 g) and 1,3,5-triaza-7-phosphadaamantane (1.000 mmol, 0.157 g) were dissolved in CH_3CN (30 mL)

and the reaction was stirred for 2 h at room temperature. Then, the ligand HL^{BSMe} (0.500 mmol, 0.113 g) was added, and the reaction was stirred for 24 h at room temperature. The precipitate obtained was filtered and dried at reduced pressure giving the complex [Cu(HL^{BSMe})(PTA)₂](PF₆) in 66% yield. M.p.: 191–193 °C. Solubility: CH₃CN, DMSO. FT-IR (cm^{−1}): 3200vbr (OH); 3062w, 3034w, 3268wbr, 2919wbr, 2879w (C-H); 1618m, 1574w (C=C and C=N); 1496w, 1449m, 1415w, 1376w, 1350w, 1294m, 1239m, 1161w, 1130w, 1107w, 1055w, 1040s, 969s, 949s, 895w; 831vs (PF₆); 742vs, 733s, 698s, 639m, 583s, 556vs, 525m, 501m. ¹H-NMR (CD₃CN, 293K): δ 2.47 (s, 3H, CH₃), 4.09 (s, 12H, NCH₂P), 4.50–4.61 (AB q, 12H, NCH₂N), 4.83 (s, 2H, CH₂), 6.82–7.71 (m, 9H, CH_{ar}), 16.25 (sbr, 1H, OH). ³¹P{¹H}-NMR (CD₃CN, 293K): δ −144.62 (septet, J_{P-F} = 706 Hz), −91.64 (sbr). ESI-MS(+) (major positive ions, CH₃CN), *m/z* (%): 226 (100) [HL^{BSMe} + H]⁺, 287 (20) [Cu(HL^{BSMe})]⁺, 377 (10) [Cu(PTA)₂]⁺, 445 (100) [Cu(HL^{BSMe})(PTA)]⁺. ESI-MS(−) (major negative ions, CH₃CN), *m/z* (%): 145 (100) [PF₆][−]. Elemental analysis (%) calculated for C₂₇H₃₉CuF₆N₇OP₃: C 43.35, H 5.25, N 13.11; found: C 44.14, H 5.39, N 13.05

3.2.4. Synthesis of [Ag(HL^{BSMe})(PTA)]NO₃ (4)

Silver nitrate (0.500 mmol, 0.085 g) and 1,3,5-triaza-phosphadaamantane (0.500 mmol, 0.078 g) were dissolved in CH₃OH (30 mL) and the reaction was stirred for 2 h at room temperature. Afterwards, the ligand HL^{BSMe} (0.500 mmol, 0.113 g) was added, the reaction was stirred at room temperature for 24 h, then the solution was evaporated under reduced pressure. The product [Ag(HL^{BSMe})(PTA)]NO₃ was obtained in 58% yield. M.p.: 206–208 °C. Solubility: CH₃OH, CH₂Cl₂, CHCl₃, CH₃CN, DMSO. FT-IR (cm^{−1}): 3210br (OH); 3060w, 3033w, 2917w, 2878w (C-H); 1616m, 1573w (C=C and C=N); 1494w; 1449m, 1425m, 1375m, 1334s, 1292s (NO₃); 1240s, 1161m, 1129w, 1107m, 1074w, 1042w, 1013vs, 970vs, 947vs, 929m, 900m, 861w, 829w, 806s, 790sh, 743vs, 732vs, 698vs, 639m, 602s, 583s, 560s, 525m, 501m. ¹H-NMR (DMSO-d₆, 293K): δ 2.48 (s, 3H, CH₃), 4.15 (s, 6H, NCH₂P), 4.41–4.58 (AB q, 6H, NCH₂N), 4.83 (s, 2H, CH₂), 6.77–7.72 (m, 9H, CH_{ar}), 16.38 (s, 1H, OH). ³¹P{¹H}-NMR (DMSO-d₆, 293K): δ −86.03 (s). ³¹P{¹H}-NMR (CDCl₃, 293K): δ −93.60 (s). ³¹P{¹H}-NMR (CD₃OD, 233K): δ −82.00 (sbr). ESI-MS(+) (major positive ions, CH₃OH), *m/z* (%): 226 (100) [HL^{BSMe} + H]⁺, 248 (20) [HL^{BSMe} + Na]⁺, 423 (50) [Ag(PTA)₂]⁺, 491 (40) [Ag(HL^{BSMe})(PTA)]⁺. ESI-MS(−) (major negative ions, CH₃OH), *m/z* (%): 145 (100) [AgNO₃ + NO₃][−]. Elemental Analysis (%) calculated for C₂₁H₂₇AgN₅O₄P: C 45.67, H 4.93, N 12.68; found: C 46.15, H 5.12, N 13.31.

3.2.5. Synthesis of [Cu(L^{BSMe})₂] (5)

Copper(II) acetate (0.250 mmol, 0.045 g) and the ligand HL^{BSMe} (0.500 mmol, 0.113 g) were solubilized in CH₃OH (20 mL). The reaction was stirred at reflux for 4 h, giving a small amount of a dark green precipitate. After filtration, the mother liquors were dried at reduced pressure obtaining the green–blue solid [Cu(L^{BSMe})₂] in 39% yield. M.p.: 201–203 °C. Solubility: CH₃OH, CH₃CN, CH₂Cl₂, CHCl₃, DMSO. FT-IR (cm^{−1}): 3083w, 3058w, 3021w, 2974w, 2904w (C-H); 1597s, 1588s (C=C and C=N); 1536s; 1494m, 1469m, 1437s, 1366w, 1328s, 1262m, 1246m, 1215m, 1159m, 1132m, 1084w, 1055m, 1046m, 933m, 856m, 756s, 742s, 705s, 695s, 649m, 602m, 570m. ESI-MS(+) (major positive ions, CH₃CN), *m/z* (%): 226 (100) [HL^{BSMe} + H]⁺, 287 (40) [Cu(L^{BSMe})]⁺, 329 (30) [Cu(L^{BSMe}) + CH₃CN]⁺, 511 (90) [Cu(L^{BSMe})₂ + H]⁺, 576 (80) [Cu(L^{BSMe})₂ + Na + CH₃CN]⁺. ESI-MS(−) (major negative ions, CH₃CN), *m/z* (%): 240 (100) [L^{BSMe}][−]. Elemental analysis (%) calculated for C₃₀H₂₈CuN₂O₂: C 70.36, H 5.51, N 5.47; found: C 69.79, H 5.41, N 5.25.

3.2.6. Synthesis of [Cu(HL^{BSPH})(PPh₃)₂](PF₆·2CH₃CN) (6)

Tetrakis(acetonitrile)copper(I)hexafluorophosphate (0.500 mmol, 0.186 g) and triphenylphosphine (1.000 mmol, 0.262 g) were dissolved in CH₃CN (30 mL) and the reaction was

stirred for 3 h at room temperature. The ligand HL^{BSPH} (0.500 mmol, 0.144 g) was added, and the reaction was stirred for 24 h at room temperature. The solvent was removed at reduced pressure and the solid obtained was washed with Et₂O. A precipitate was recovered by filtration giving the complex [Cu(HL^{BSPH})₂(PPh₃)]PF₆·2CH₃CN in 83% yield. M.p.: 161–164 °C. Solubility: CH₃OH, CH₃CN, CHCl₃, CH₂Cl₂, DMSO. FT-IR (cm^{−1}): 3070w, 3050w, 3028w, 2938w, 2916w (C-H); 2301wbr, 2271wbr (CH₃CN); 1605m, 1572w (C=C and C=N); 1497w, 1480m, 1450w, 1434s, 1369w, 1346w, 1328w, 1304m, 1258m, 1245w, 1181w, 1150w, 1112w, 1095m, 1072w, 1047w, 1035w, 999w, 972w, 923w, 879w, 859msh; 832vs (PF₆); 775m, 766m, 744vs, 716m, 694vs, 646m, 618w, 557vs, 541m, 527m, 516s, 504vs. ¹H-NMR (CD₃CN 293K): δ 1.99 (s, 6H, CH₃CN), 4.55 (s, 2H, CH₂), 6.71–7.69 (m, 44H, CH_{ar}), 15.41 (s, 1H, OH). ¹H-NMR (CDCl₃ 293K): δ 2.08 (s, 6H, CH₃CN), 4.61 (s, 2H, CH₂), 6.70–7.71 (m, 44H, CH_{ar}). ³¹P{¹H}-NMR (CD₃CN, 293K): δ −144.62 (septet, J_{P-F} = 706 Hz), −0.30 (sbr). ³¹P{¹H}-NMR (CDCl₃, 293K): δ −144.25 (septet, J_{P-F} = 713 Hz), −0.61 (s). ESI-MS(+) (major positive ions, CH₃CN), *m/z* (%): 366 (100) [Cu(PPh₃) + CH₃CN]⁺, 589 (100) [Cu(PPh₃)₂]⁺. ESI-MS(−) (major negative ions, CH₃CN), *m/z* (%): 145 (100) [PF₆][−]. Elemental Analysis (%) calculated for C₆₀H₅₃CuF₆N₃OP₃: C 65.36, H 4.85, N 3.81; found: C 65.25, H 4.88, N 3.66.

3.2.7. Synthesis of [Cu(HL^{BSPH})(PTA)₂](PF₆)·2H₂O (7)

Tetrakis(acetonitrile)copper(I)hexafluorophosphate (0.500 mmol, 0.186 g) and 1,3,5-triaza-7-phosphadaamantane (1.000 mmol, 0.157 g) were dissolved in CH₃CN (30 mL) and the reaction was stirred for 2 h at room temperature. The ligand HL^{BSPH} (0.500 mmol, 0.144 g) was added giving a yellow mixture. After 24 h at room temperature, the solvent was evaporated under reduced pressure obtaining the complex [Cu(HL^{BSPH})(PTA)₂](PF₆)·2H₂O in 72% yield. M.p.: 225–228 °C. Solubility: CH₃OH, CH₃CH₂OH, CH₂Cl₂, CHCl₃, CH₃CN, DMSO. FT-IR (cm^{−1}): 3345wbr, 3188wbr (OH); 3063wbr, 3028w, 2916w, 2878w (C-H); 1605s, 1571m (C=C and C=N); 1497m, 1441m, 1419m; C=N; 1346w, 1328w, 1303m, 1257m, 1242s, 1171w, 1150m, 1111m, 1081w, 1045w, 1015s, 970s, 949s, 923m, 876w; 832vs (PF₆); 775s, 765s, 751vs, 715vs, 698vs, 646s, 611m, 582s, 555vs, 506s. ¹H-NMR (CD₃CN, 293K): δ 2.24 (s, 4H, H₂O), 4.08 (s, 12H, NCH₂N), 4.50–4.60 (AB q, 14H, NCH₂P and CH₂), 6.70–7.62 (m, 14H, CH_{ar}), 15.45 (s, 1H, OH). ³¹P{¹H}-NMR (CD₃CN, 293K): δ −144.58 (septet, J_{P-F} = 706 Hz), −89.66 (br). ESI-MS(+) (major positive ions, CH₃CN), *m/z* (%): 261 (90) [Cu(PTA) + CH₃CN]⁺, 288 (20) [HL^{BSPH} + H]⁺, 377 (10) [Cu(PTA)₂]⁺, 507 (15) [Cu(HL^{BSPH})(PTA)]⁺. ESI-MS(−) (major negative ions, CH₃CN), *m/z* (%): 145 (100) [PF₆][−]. Elemental Analysis (%) calculated for C₃₂H₄₅CuF₆N₇O₃P₃: C 45.42, H 5.36, N 11.59; found: C 44.69, H 5.03, N 12.24.

3.2.8. Synthesis of [Ag(HL^{BSPH})(PPh₃)₂](NO₃) (8)

Silver nitrate (0.500 mmol, 0.085 g) and triphenylphosphine (1.000 mmol, 0.262 g) were dissolved in CH₃CN (30 mL) and the reaction was stirred for 2 h at room temperature. Afterwards, the ligand HL^{BSPH} (0.500 mmol, 0.144 g) was added, and the reaction was stirred at room temperature for 24 h. The precipitate obtained was filtered and dried under reduced pressure giving the product [Ag(HL^{BSPH})(PPh₃)₂](NO₃) in 40% yield. M.p.: 187–189 °C. Solubility: CH₃OH, CH₂Cl₂, CHCl₃, CH₃CN. FT-IR (cm^{−1}): 3059wbr, 3028w, 2918w (C-H); 1605m, 1571w (C=C and C=N); 1497w, 1489w; 1479m, 1436m, 1397s, 1346w, 1328w, 1296s (NO₃); 1257m, 1179w, 1150m, 1112w, 1095m, 1072w, 1047m, 1025m, 997m, 971w, 918s, 864w, 849w, 833w, 825w, 818w, 775m, 766m, 751vs, 742vs, 715s, 693vs, 646m, 618w, 567w, 547w, 513ssh, 503vs. ¹H-NMR (CDCl₃, 293K): δ 4.58 (s, 2H, CH₂), 6.68–7.70 (m, 44H, CH_{ar}), 15.67 (s, 1H, OH). ¹H-NMR (DMSO-d₆, 293K): δ 4.52 (s, 2H, CH₂), 6.71–7.63 (m, 44H, CH_{ar}), 15.46 (s, 1H, OH). ³¹P{¹H}-NMR (CDCl₃, 293K): δ 14.68 (sbr). ³¹P{¹H}-NMR (CD₃CN, 233K): δ 8.69 (d, J(Ag-³¹P) = 478 Hz). ESI-MS(+) (major positive ions, CH₃CN), *m/z* (%): 288 (10) [HL^{BSPH} + H]⁺, 371 (30) [Ag(PPh₃)]⁺, 410 (30) [Ag(PPh₃) + CH₃CN]⁺, 630

(100) $[\text{Ag}(\text{PPh}_3)_2]^+$. ESI-MS(−) (major negative ions, CH_3OH), m/z (%): 231 (100) $[\text{AgNO}_3 + \text{NO}_3]^-$. Elemental analysis (%) calculated for $\text{C}_{56}\text{H}_{47}\text{AgN}_2\text{O}_4\text{P}_2$: C 68.51, H 4.83, N 2.85; found: C 69.43, H 4.87, N 2.90.

3.2.9. Synthesis of $[\text{Ag}(\text{HL}^{\text{BSPH}})(\text{PTA})]\text{NO}_3$ (9)

Silver nitrate (0.500 mmol, 0.085 g) and 1,3,5-triaza-7-phosphadaamantane (0.500 mmol, 0.078 g) were dissolved in CH_3CN . After 2 h, the ligand HL^{BSPH} (0.500 mmol, 0.145 g) was added and the reaction was stirred at room temperature for 22 h and refluxed for further 4 h. Successively, the solvent was removed under reduced pressure and the yellow solid product $[\text{Ag}(\text{HL}^{\text{BSPH}})(\text{PTA})]\text{NO}_3$ was obtained in 55% yield. M.p.: 232–234 °C. Solubility: CH_3OH , CH_3CN , CHCl_3 , CH_2Cl_2 , DMSO. FT-IR (cm^{-1}): 3200wbr (OH); 3064wbr, 3029w, 2916w (C-H); 1605s, 1571m (C=C and C=N); 1516w, 1497w, 1489w; 1450m, 1441m, 1425m, 1416m, 1374m, 1329s, 1294s (NO_3); 1257s, 1241s, 1170w, 1150m, 1110m, 1081w, 1072w, 1045m, 1013s, 970vs, 947vs, 919s, 865w, 851m, 825m, 775s, 766s, 751vs, 715vs, 698vs, 646s, 605s, 582s, 564s, 547m, 506s. ^1H -NMR ($\text{DMSO}-d_6$, 293K): δ 4.16 (s, 6H, NCH_2N), 4.42–4.58 (dd, 6H, NCH_2P and CH_2), 6.71–7.63 (m, 14H, CH_{ar}), 15.45 (sbr, 1H, OH). $^{31}\text{P}\{^1\text{H}\}$ -NMR (CDCl_3 , 293K): δ −94.43 (s). $^{31}\text{P}\{^1\text{H}\}$ -NMR (CD_3CN , 233K): δ −86.09 (sbr). ESI-MS(+) (major positive ions, CH_3CN), m/z (%): 158 (90) $[\text{PTA} + \text{H}]^+$, 260 (80) $[\text{Ag}(\text{PTA})]^+$, 288 (100) $[\text{HL}^{\text{BSPH}} + \text{H}]^+$, 423 (50) $[\text{Ag}(\text{PTA})_2]^+$, 553 (10) $[\text{Ag}(\text{HL}^{\text{BSPH}})(\text{PTA})]^+$. ESI-MS(−) (major negative ions, CH_3CN), m/z (%): 231 (70) $[\text{AgNO}_3 + \text{NO}_3]^-$. Elemental analysis (%) calculated for $\text{C}_{26}\text{H}_{27}\text{AgN}_5\text{O}_4\text{P}$: C 50.83, H 4.76, N 11.50; found: C 51.27, H 5.12, N 11.91.

3.2.10. Synthesis of $[\text{Cu}(\text{L}^{\text{BSPH}})_2]$ (10)

Copper(II) acetate (1.000 mmol, 0.200 g) was dissolved in CH_3OH obtaining an intense blue solution. At the same time, the ligand HL^{BSPH} (2.000 mmol, 0.115 g) was solubilized in CH_3CN . The two solutions were mixed, and it was stirred at room temperature for 1 h and then refluxed for 23 h. After 24 h, the dark green precipitate formed was filtered and dried under reduced pressure giving the complex $[\text{Cu}(\text{L}^{\text{BSPH}})_2]$ in 77% yield. A batch of good quality crystals of $[\text{Cu}(\text{L}^{\text{BSPH}})_2]$, suitable for X-ray analysis, was obtained by slow evaporation of a toluene solution of **10**. M.p.: 228–230 °C. Solubility: CH_3OH , $\text{CH}_3\text{CH}_2\text{OH}$, CH_2Cl_2 , CH_3Cl , EtOAc, CH_3CN , DMSO, Acetone. FT-IR (cm^{-1}): 3080w, 3044w, 3025w, 2940w (C-H); 1599s, 1568s (C=C and C=N); 1529vs; 1491m, 1456m, 1440vs, 1341vs, 1257s, 1241s, 1203w, 1178w, 1142vs, 1120m, 1075m, 1051m, 1039w, 1024m, 998w, 961m, 935s, 914m, 847s, 777m, 765m, 747vs, 720s, 702vs, 691vs, 641w, 629m, 618m. ESI-MS(+) (major positive ions, CH_3CN), m/z (%): 288 (100) $[\text{HL}^{\text{BSPH}} + \text{H}]^+$, 349 (70) $[\text{Cu}(\text{L}^{\text{BSPH}})]^+$, 390 (100) $[\text{Cu}(\text{L}^{\text{BSPH}}) + \text{CH}_3\text{CN}]^+$, 636 (20) $[2\text{HL}^{\text{BSPH}} + \text{H}]^+$, 658 (20) $[2\text{HL}^{\text{BSPH}} + \text{Na}]^+$, 741 (25) $[2\text{HL}^{\text{BSPH}} + \text{Na} + 2\text{CH}_3\text{CN}]^+$. Elemental analysis (%) calculated for $\text{C}_{40}\text{H}_{32}\text{CuN}_5\text{O}_5$: C 75.51, H 5.07, N 4.40; found: C 75.38, H 5.12, N 4.41.

3.3. Crystallographic Data Collection and Refinement

A batch of very good crystals were obtained by slow recrystallization of the $[\text{Cu}(\text{L}^{\text{BSPH}})_2]$ complex from a toluene solution. The specimens were of prismatic shape and intensely colored in green. The selected item was fixed to a glass capillary with Loctite glue and mounted on the head of a four-circle, kappa-geometry single-crystal OD Rigaku diffractometer. The data collection was performed under a graphite-monochromated $\text{Cu K}\alpha$ radiation ($\lambda = 1.54184 \text{ \AA}$) at room temperature [295.1(3) K], and reflections were collected with the ω -scans technique. The preliminary screening of the sample allowed us to plan the data collection in the 1024×1024 pixel mode and 2×2 pixel binning. Intensity spots were recorded with an Atlas CCD area detector recently obtained by Prof. K Rissanen (University of Jyväskylä, Finland) in replacement of the former EOS camera. The crude diffraction data were collected working with the CrysAlisPro software, Version 1.171.43.141a [157],

and treated for Lorentz and polarization effects. An empirical correction for absorption based on a multi-scan approach using equivalent reflections was applied by means of the SCALE3 ABSPACK algorithm, also accessible via the CrysAlisPro software. Two reference frames were collected every 50 frames to ensure crystal and equipment stability, showing no sign of sample deterioration or motion.

The complex crystallizes in the monoclinic system and the structure was solved in the $I2/a$ space group; the unit cell parameters have been refined by working on the least-squares refinement of 18,133 strong reflections gathered during the whole experiment. The structure solution was performed by direct phasing and refined by full-matrix least-squares methods based on F_o^2 through the OLEX2 program interface [158] with the SHELXT and SHELXL [159,160] programs. The asymmetric unit contains half of a molecule, with the copper ion lying on a proper two-fold axis, and the whole cell hosts four units of the complex, which are very efficiently packed (no solvent accessible voids). In the final stages of the refinement, non-H atoms were allowed to vibrate anisotropically, whereas the H atoms were placed in calculated positions and refined as a riding model, with their displacement parameters calculated as 1.2 times the U_{eq} of the ‘parent’ atom.

At this level, it turned out that the phenyl ring (C15/C20) belonging to the benzylimino moiety of the ligand can assume two possible arrangements (involved atoms labelled with a final ‘A’). The sum of the pertinent occupation factors for each disordered position were constrained to unity, with finally refined sofs of 0.57/0.43 for untagged and tagged atoms, respectively. A regular hexagon geometry with bond distances of 1.3900 Å was imposed on the disordered positions of the phenyl ring via the AFIX 6 constraint to ensure refinement convergence and to prevent some atoms from assuming non-positive definite displacement parameters. A summary of crystal and data collection parameters is given below in Table 4; full listings of bond lengths and angles are in Tables S2 and S3. Representations of the asymmetric unit of $[Cu(L^{BSPH})_2]$ and of the entire complex (Figures 1 and 2) with and without the disordered rings, highlighting the selected numbering scheme, have been prepared with the Mercury 4.2.0 software [161]. Complete listings of atomic coordinates, bond lengths, bond angles, and anisotropic thermal parameters are available as supporting information, in the form of the .cif file, that has been deposited at the Cambridge Crystallographic Data Center (CCDC) with deposition number 2433689. These data can be obtained free of charge via www.ccdc.cam.ac.uk/structures (accessed on 21 April 2025).

Table 4. Summary of crystal and data collection parameters for $[Cu(L^{BSPH})_2]$ (10).

Empirical Formula	$C_{40}H_{32}CuN_2O_2$
Formula weight	636.21
Temperature/K	295.1(3)
Radiation	Cu K α (λ = 1.54184)
Crystal system	monoclinic
Space group	$I2/a$
$a/\text{\AA}$	20.4267(4)
$b/\text{\AA}$	8.7751(2)
$c/\text{\AA}$	18.3240(3)
$\alpha/^\circ$	90
$\beta/^\circ$	101.135(2)
$\gamma/^\circ$	90
Volume/ \AA^3	3222.68(11)
Z	4
$\rho_{\text{calc}} \text{ g/cm}^3$	1.311
μ/mm^{-1}	1.246
$F(000)$	1324.0

Table 4. Cont.

Empirical Formula	C ₄₀ H ₃₂ CuN ₂ O ₂
Crystal size/mm ³	0.42 × 0.4 × 0.2
2θ range for data collection/°	8.824 to 155.422
Index ranges	−20 ≤ h ≤ 25, −11 ≤ k ≤ 11, −23 ≤ l ≤ 23
Reflections collected	36,327
Independent reflections	3416 [R _{int} = 0.0377]
Data/restraints/parameters	3416/0/247
Goodness-of-fit on F ²	1.034
Final R indexes [I ≥ 2σ(I)]	R ₁ = 0.0331, wR ₂ = 0.0927
Largest diff. peak/hole/e Å ^{−3}	0.17/−0.31

Goodness-of-fit = $[\sum (w(F_o^2 - F_c^2)^2) / (N_{\text{obsvns}} - N_{\text{params}})]^{1/2}$, based on all data; $R_1 = \sum ||F_o| - |F_c|| / \sum |F_o|$; $wR_2 = [\sum w(F_o^2 - F_c^2)^2 / \sum w(F_o^2)^2]^{1/2}$.

3.4. Antibacterial Screening

The synthesized Schiff bases HL^{BSMe} (1) and HL^{BSP^h} (2), the related metal complexes 3–10, and the free phosphane co-ligands triphenylphosphine (11) and, 3,5-triaza-7-phosphadaamantane (12), were evaluated for their in-vitro antibacterial activity against Gram-negative (*Escherichia coli* China-bio-00021) and Gram-positive bacteria (*Staphylococcus aureus* ATCC 25923), with ciprofloxacin serving as standard antibacterial agent. The antimicrobial properties of the compounds were evaluated using the standard broth microdilution method in 96-well cell culture plates following the reported method [162]. Firstly, the compounds were dissolved in PBS buffer containing 1% DMSO solution and stirred for 20 min until forming the homogeneous suspension (1.0 mg mL^{−1}). Subsequently, a series of compounds solutions (50 µL) were prepared in a 96-well plate using the double dilution method, followed by the addition of bacterial suspensions. The final compound concentrations were 3.125, 6.25, 12.5, 25, 50, 100, and 200 µg mL^{−1}, and the final bacterial concentration was 5 × 10⁶ CFU mL^{−1}. The group without an antimicrobial agent was set as the control. Then, the 96-well plate was incubated at 37 °C for 24 h and the optical density (OD₆₀₀) values of each well was recorded at different times (0, 2, 4, 6, 8, 10, 12, 20, and 24 h) using a microplate reader (Thermo Scientific, Waltham, MA, USA). According to the principle that the turbidity of the culture increases with the proliferation of bacteria, the growth state of bacteria can be evaluated by detecting the absorbance value of the bacterial suspension at 600 nm. In addition, the synthesized compounds were evaluated for their in-vitro antibacterial activity against two bacterial strains using the plate count method. Typically, 100 µL of bacterial suspension (10⁶ CFU mL^{−1}) was mixed with 100 µL of compound solution at different concentrations (25, 50, 100, 200 and 400 µg mL^{−1}). Subsequently, 100 µL of the mixed solution was spread on LB agar plates. After incubation at 37 °C for another 24 h, the surviving bacteria on each plate were counted. The antibacterial ratio was calculated using the following formula, where C_b and C_e are the numbers of colonies in the blank group and the experimental group, respectively, as follows:

$$\text{Antibacterial efficiency} = \frac{C_b - C_e}{C_b} \times 100\%$$

Statistical Analysis

The collected data were analyzed using GraphPad Prism 10 or OriginPro 2021 (9.8) software. Statistical significance was defined as $p < 0.05$, and the results were presented to three decimal places.

4. Conclusions

In this study, we report the synthesis, characterization, and antibacterial evaluation of Cu(I) and Ag(I) complexes supported by two phenoxy-ketimines ligands. In particular, 2-(1-(benzylimino)ethyl)phenol (HL^{BSMe}) and 2-((benzylimino)(phenyl)methyl)phenol (HL^{B^{SP}h}), characterized by the presence of methyl or phenyl substituents on the imine group, were employed for the preparation of the complexes 2–4 and 6–9, using the lipophilic PPh₃ and the hydrophilic PTA as co-ligands to stabilize the metal in +1 oxidation state. The analogous copper(II) complexes 5 and 10 were synthesized using the copper(II) acetate salt Cu(CH₃COO)₂ and the ligands HL^{BSMe} and HL^{B^{SP}h}, respectively. All species were fully characterized both in the solid state and in solution. The single-crystal XRD allowed us to describe the molecular structure of 10, the first reported complex of Cu(II) with the HL^{B^{SP}h} ligand, where the copper ion has a slightly distorted square planar environment, as well as to highlight the efficient crystal packing, even in the absence of strong canonical hydrogen bonds, largely driven by $\pi \cdots \pi$ and C–H $\cdots \pi$ nonbonding interactions. The antimicrobial properties of the new copper and silver complexes as well as of the corresponding uncoordinated ligands were evaluated against *E. coli* and *S. aureus*. The results revealed that all the complexes exhibited moderate to excellent antibacterial efficacy. Among them, the Ag(I) complexes displayed the highest antibacterial activity. Specifically, [Ag(HL^{B^{SP}h})(PTA)]NO₃ demonstrated the most promising antibacterial performance, with MIC values of 0.025 and 0.05 mg mL^{−1} against *E. coli* and *S. aureus*, respectively, while the corresponding MBC values were 0.100 and 0.200 mg mL^{−1}.

This study provides new insights into the design of antimicrobial agents, highlighting the potential for rationally designing and synthesizing novel, highly efficient antibacterial compounds. To further enhance the antibacterial activity of the silver complexes of phenoxy-ketimine Schiff base ligands, future research should focus on optimizing the synthesis of the most promising candidates, including fine-tuning the electronic and steric effects of both primary and auxiliary ligands, as well as modifying the solubility properties of the related complexes. In addition, detailed mechanistic studies could reveal specific pathways and interactions, facilitating the design of more effective compounds. Future investigations should also prioritize an in-depth exploration of structure-activity relationships to elucidate the role of distinctive phosphanes and of different substituents on the phenoxy-ketimines ligands in biological activity.

Supplementary Materials: The following supporting information can be downloaded at: <https://www.mdpi.com/article/10.3390/molecules30091893/s1>, Figures S1–S35: FT-IR, ¹H-, ¹³C-, and ³¹P-NMR spectra of compounds 1–10; Figures S36–S38: packing diagrams highlighting nonbonding interaction network for complex 10; Table S1: ¹H- and ³¹P{¹H}-NMR selected data; Tables S2 and S3: full listings of bond lengths and angles of the complex 10.

Author Contributions: Conceptualization, C.S. and M.P.; data curation, M.C., Z.L., J.D.G. and A.D.; formal analysis, M.C., Z.L., J.D.G. and A.D.; investigation, M.C., Z.L., C.C. and M.P.; methodology, M.C., Z.L., J.D.G., A.D. and M.P.; supervision, C.C., M.D. and M.P.; writing—original draft, Z.L., C.S., M.D., A.D. and M.P. All authors have read and agreed to the published version of the manuscript.

Funding: This research was funded by Unione Europea—NextGenerationEU (MUR-Fondo Promozione e Sviluppo—D.M. 737/2021, INVIRCUM, University of Camerino, FAR 2022 PNR, and NGEU PNRR, D.M. n. 351/2022 M4C1 I4.1) and by the University of Padova (PRID BIRD225980).

Institutional Review Board Statement: Not applicable.

Informed Consent Statement: Not applicable.

Data Availability Statement: The data presented in this study are available on request from the corresponding authors. CCDC 2433689 contains the supplementary crystallographic data for this paper, available free of charge from the Cambridge Crystallographic Data Centre via www.ccdc.cam.ac.uk/structures (accessed on 21 April 2025).

Conflicts of Interest: The authors declare no conflicts of interest.

References

1. Hofer, U. The cost of antimicrobial resistance. *Nat. Rev. Microbiol.* **2019**, *17*, 3. [CrossRef] [PubMed]
2. World Health Organization. WHO Bacterial Priority Pathogens List, 2024: Bacterial Pathogens of Public Health Importance to Guide Research, Development and Strategies to Prevent and Control Antimicrobial Resistance. Available online: <https://www.who.int/publications/i/item/9789240093461> (accessed on 1 November 2024).
3. World Health Organization. WHO Publishes List of Bacteria for Which New Antibiotics Are Urgently Needed. Available online: <https://www.who.int/en/news-room/detail/27-02-2017-who-publishes-list-of-bacteria-for-which-new-antibiotics-are-urgently-needed> (accessed on 1 November 2024).
4. Frei, A.; Verderosa, A.D.; Elliott, A.G.; Zuegg, J.; Blaskovich, M.A.T. Metals to combat antimicrobial resistance. *Nat. Rev. Chem.* **2023**, *7*, 202–224. [CrossRef] [PubMed]
5. Ruggieri, F.; Compagne, N.; Antraygues, K.; Eveque, M.; Flipo, M.; Willand, N. Antibiotics with novel mode of action as new weapons to fight antimicrobial resistance. *Eur. J. Med. Chem.* **2023**, *256*, 115413. [CrossRef] [PubMed]
6. Miethke, M.; Pieroni, M.; Weber, T.; Brönstrup, M.; Hammann, P.; Halby, L.; Arimondo, P.B.; Glaser, P.; Aigle, B.; Bode, H.B.; et al. Towards the sustainable discovery and development of new antibiotics. *Nat. Rev. Chem.* **2021**, *5*, 726–749. [CrossRef]
7. Lin, Y.; Betts, H.; Keller, S.; Cariou, K.; Gasser, G. Recent developments of metal-based compounds against fungal pathogens. *Chem. Soc. Rev.* **2021**, *50*, 10346–10402. [CrossRef]
8. Collignon, P.; Beggs, J.J.; Walsh, T.R.; Gandra, S.; Laxminarayan, R. Anthropological and socioeconomic factors contributing to global antimicrobial resistance: A univariate and multivariable analysis. *Lancet Planetary Health* **2018**, *2*, E398–E405. [CrossRef]
9. Barry, N.P.E.; Sadler, P.J. Exploration of the medical periodic table: Towards new targets. *Chem. Commun.* **2013**, *49*, 5106–5131. [CrossRef]
10. Mjos, K.D.; Orvig, C. Metallodrugs in Medicinal Inorganic Chemistry. *Chem. Rev.* **2014**, *114*, 4540–4563. [CrossRef]
11. Cvijan, B.B.; Jacic, J.K.; Bajcetic, M. The Impact of Copper Ions on the Activity of Antibiotic Drugs. *Molecules* **2023**, *28*, 5133. [CrossRef]
12. Frei, A.; Zuegg, J.; Elliott, A.G.; Baker, M.; Braese, S.; Brown, C.; Chen, F.; Dowson, C.G.; Dujardin, G.; Jung, N.; et al. Metal complexes as a promising source for new antibiotics. *Chem. Sci.* **2020**, *11*, 2627–2639. [CrossRef]
13. Ghanghas, P.; Choudhary, A.; Kumar, D.; Poonia, K. Coordination metal complexes with Schiff bases: Useful pharmacophores with comprehensive biological applications. *Inorg. Chem. Commun.* **2021**, *130*, 108710. [CrossRef]
14. Alkis, M.E.; Kelestemür, Ü.; Alan, Y.; Turan, N.; Buldurun, K. Cobalt and ruthenium complexes with pyrimidine based Schiff base: Synthesis, characterization, anticancer activities and electrochemotherapy efficiency. *J. Mol. Struct.* **2021**, *1226*, 129402. [CrossRef]
15. More, M.S.; Joshi, P.G.; Mishra, Y.K.; Khanna, P.K. Metal complexes driven from Schiff bases and semicarbazones for biomedical and allied applications: A review. *Mater. Today Chem.* **2019**, *14*, 100195. [CrossRef] [PubMed]
16. Magyari, J.; Holló, B.B.; Vojinovic-Jesic, L.S.; Radanovic, M.M.; Armakovic, S.; Armakovic, S.J.; Molnár, J.; Kincses, A.; Gajdács, M.; Spengler, G.; et al. Interactions of Schiff base compounds and their coordination complexes with the drug cisplatin. *New J. Chem.* **2018**, *42*, 5834–5843. [CrossRef]
17. Al Zoubi, W.; Al-Hamdani, A.A.S.; Kaseem, M. Synthesis and antioxidant activities of Schiff bases and their complexes: A review. *Appl. Organomet. Chem.* **2016**, *30*, 810–817. [CrossRef]
18. Al Zoubi, W.; Ko, Y.G. Organometallic complexes of Schiff bases: Recent progress in oxidation catalysis. *J. Organomet. Chem.* **2016**, *822*, 173–188. [CrossRef]
19. Jia, Y.; Li, J.B. Molecular Assembly of Schiff Base Interactions: Construction and Application. *Chem. Rev.* **2015**, *115*, 1597–1621. [CrossRef]
20. Qin, W.L.; Long, S.; Panunzio, M.; Biondi, S. Schiff Bases: A Short Survey on an Evergreen Chemistry Tool. *Molecules* **2013**, *18*, 12264–12289. [CrossRef]
21. Gupta, K.C.; Sutar, A.K. Catalytic activities of Schiff base transition metal complexes. *Coord. Chem. Rev.* **2008**, *252*, 1420–1450. [CrossRef]
22. Nakayama, Y.; Saito, J.; Bando, H.; Fujita, T. Propylene Polymerization Behavior of Fluorinated Bis(phenoxy-imine) Ti Complexes with an MgCl₂-Based Compound (MgCl₂-Supported Ti-Based Catalysts). *Macromol. Chem. Phys.* **2005**, *206*, 1847–1852. [CrossRef]
23. Vigato, P.A.; Tamburini, S. The challenge of cyclic and acyclic Schiff bases and related derivatives. *Coord. Chem. Rev.* **2004**, *248*, 1717–2128. [CrossRef]

24. Cozzi, P.G. Metal-Salen Schiff base complexes in catalysis: Practical aspects. *Chem. Soc. Rev.* **2004**, *33*, 410–421. [[CrossRef](#)] [[PubMed](#)]
25. Akitsu, T. *Novelties in Schiff Bases*; IntechOpen: London, UK, 2024; p. 160.
26. Younus, H.A.; Saleem, F.; Hameed, A.; Al-Rashida, M.; Al-Qawasmeh, R.A.; El-Naggar, M.; Rana, S.; Saeed, M.; Khan, K.M. Part-II: An update of Schiff bases synthesis and applications in medicinal chemistry-a patent review (2016–2023). *Expert Opin. Ther. Patents* **2023**, *33*, 841–864. [[CrossRef](#)] [[PubMed](#)]
27. Nath, B.D.; Islam, M.M.; Karim, M.R.; Rahman, S.; Shaikh, M.A.A.; Georghiou, P.E.; Menelaou, M. Recent Progress in Metal-Incorporated Acyclic Schiff-Base Derivatives: Biological Aspects. *ChemistrySelect* **2022**, *7*, e202104290. [[CrossRef](#)]
28. Soroceanu, A.; Bargan, A. Advanced and Biomedical Applications of Schiff-Base Ligands and Their Metal Complexes: A Review. *Crystals* **2022**, *12*, 1436. [[CrossRef](#)]
29. Omid, S.; Kakanejadifard, A. A review on biological activities of Schiff base, hydrazone, and oxime derivatives of curcumin. *RSC Adv.* **2020**, *10*, 30186–30202. [[CrossRef](#)]
30. Parveen, S. Recent advances in anticancer ruthenium Schiff base complexes. *Appl. Organomet. Chem.* **2020**, *34*, e5687. [[CrossRef](#)]
31. Khan, A.M.; Abid, O.U.R.; Mir, S. Assessment of biological activities of chitosan Schiff base tagged with medicinal plants. *Biopolymers* **2020**, *111*, e23338. [[CrossRef](#)]
32. Hameed, A.; al-Rashida, M.; Uroos, M.; Ali, S.A.; Khan, K.M. Schiff bases in medicinal chemistry: A patent review (2010–2015). *Expert Opin. Ther. Patents* **2017**, *27*, 63–79. [[CrossRef](#)]
33. Nayab, P.S.; Akrema; Ansari, I.A.; Shahid, M.; Rahisuddin. New phthalimide-appended Schiff bases: Studies of DNA binding, molecular docking and antioxidant activities. *Luminescence* **2017**, *32*, 829–838. [[CrossRef](#)]
34. Przybylski, P.; Huczynski, A.; Pyta, K.; Brzezinski, B.; Bartl, F. Biological Properties of Schiff Bases and Azo Derivatives of Phenols. *Curr. Org. Chem.* **2009**, *13*, 124–148. [[CrossRef](#)]
35. Lv, L.; Zheng, T.P.; Tang, L.; Wang, Z.R.; Liu, W.K. Recent advances of Schiff base metal complexes as potential anticancer agents. *Coord. Chem. Rev.* **2025**, *525*, 216327. [[CrossRef](#)]
36. Kadhum, A.M.; Mallah, S.H.; Waheeb, A.S.; Salman, A.W.; Zafar, A.; Ahmad, N.S.; Siraj, S.; Iqbal, M.A. Advancement in Schiff base complexes for treatment of colon cancer. *Rev. Inorg. Chem.* **2024**, 1–21. [[CrossRef](#)]
37. Thakur, S.; Jaryal, A.; Bhalla, A. Recent advances in biological and medicinal profile of Schiff bases and their metal complexes: An updated version (2018–2023). *Results Chem.* **2024**, *7*, 101350. [[CrossRef](#)]
38. Jorge, J.; Santos, K.F.D.; Timoteo, F.; Vasconcelos, R.R.P.; Caceres, O.I.A.; Granja, I.J.A.; De Souza, D.M., Jr.; Frizon, T.E.A.; Botteselle, G.D.; Braga, A.L.; et al. Recent Advances on the Antimicrobial Activities of Schiff Bases and their Metal Complexes: An Updated Overview. *Curr. Med. Chem.* **2024**, *31*, 2330–2344. [[CrossRef](#)] [[PubMed](#)]
39. Ceramella, J.; Iacopetta, D.; Catalano, A.; Cirillo, F.; Lappano, R.; Sinicropi, M.S. A Review on the Antimicrobial Activity of Schiff Bases: Data Collection and Recent Studies. *Antibiotics* **2022**, *11*, 191. [[CrossRef](#)]
40. Sovari, S.N.; Zobi, F. Recent Studies on the Antimicrobial Activity of Transition Metal Complexes of Groups 6–12. *Chemistry* **2020**, *2*, 418–452. [[CrossRef](#)]
41. Malik, M.A.; Dar, O.A.; Gull, P.; Wani, M.Y.; Hashmi, A.A. Heterocyclic Schiff base transition metal complexes in antimicrobial and anticancer chemotherapy. *MedChemComm* **2018**, *9*, 409–436. [[CrossRef](#)]
42. Hassan, M.A.; Omer, A.M.; Abbas, E.; Baset, W.M.A.; Tamer, T.M. Preparation, physicochemical characterization and antimicrobial activities of novel two phenolic chitosan Schiff base derivatives. *Sci. Rep.* **2018**, *8*, 11416. [[CrossRef](#)]
43. Low, M.L.; Maigre, L.; Dorlet, P.; Guillot, R.; Pagès, J.M.; Crouse, K.A.; Policar, C.; Delsuc, N. Conjugation of a New Series of Dithiocarbamate Schiff Base Copper(II) Complexes with Vectors Selected to Enhance Antibacterial Activity. *Bioconjug. Chem.* **2014**, *25*, 2269–2284. [[CrossRef](#)]
44. da Silva, C.M.; da Silva, D.L.; Modolo, L.V.; Alves, R.B.; de Resende, M.A.; Martins, C.V.B.; de Fátima, Â. Schiff bases: A short review of their antimicrobial activities. *J. Adv. Res.* **2011**, *2*, 1–8. [[CrossRef](#)]
45. Bagihalli, G.B.; Avaji, P.G.; Patil, S.A.; Badami, P.S. Synthesis, spectral characterization, in vitro antibacterial, antifungal and cytotoxic activities of Co(II), Ni(II) and Cu(II) complexes with 1,2,4-triazole Schiff bases. *Eur. J. Med. Chem.* **2008**, *43*, 2639–2649. [[CrossRef](#)] [[PubMed](#)]
46. Ashraf, T.; Ali, B.; Qayyum, H.; Haroone, M.S.; Shabbir, G. Pharmacological aspects of Schiff base metal complexes: A critical review. *Inorg. Chem. Commun.* **2023**, *150*, 110449. [[CrossRef](#)]
47. Routaray, A.; Nath, N.; Maharana, T.; Sahoo, P.K.; Das, J.P.; Sutar, A.K. Salicylaldimine Copper(II) complex catalyst: Pioneer for ring opening Polymerization of Lactide. *J. Chem. Sci.* **2016**, *128*, 883–891. [[CrossRef](#)]
48. John, A.; Katiyar, V.; Pang, K.; Shaikh, M.M.; Nanavati, H.; Ghosh, P. Ni(II) and Cu(II) complexes of phenoxy-ketimine ligands: Synthesis, structures and their utility in bulk ring-opening polymerization (ROP) of L-lactide. *Polyhedron* **2007**, *26*, 4033–4044. [[CrossRef](#)]
49. Felemban, M.F.; Tayeb, F.J.; Alqarni, A.; Ashour, A.A.; Shafie, A. Recent advances in Schiff base coinage metal complexes as anticancer agents: A comprehensive review (2021–2025). *Dyes Pigment.* **2025**, *237*, 112710. [[CrossRef](#)]

50. Babic, S.; Marjanovic, J.S.; Divac, V.M.; Klisuric, O.R.; Milivojevic, D.; Bogojeski, J.V.; Rakovic, I.; Zaric, M.; Jovanovic, M.; Zaric, R.Z.; et al. Molecular docking study and in vitro evaluation of apoptotic effect of biogenic-amine-based N, O-Cu(II) complexes as potent antitumor agents. *J. Coord. Chem.* **2025**, *78*, 1007–1026. [\[CrossRef\]](#)
51. Richa; Kumar, V.; Kataria, R. Phenanthroline and Schiff Base associated Cu(II)-coordinated compounds containing N, O as donor atoms for potent anticancer activity. *J. Inorg. Biochem.* **2024**, *251*, 112440. [\[CrossRef\]](#) [\[PubMed\]](#)
52. Santini, C.; Pellei, M.; Gandin, V.; Porchia, M.; Tisato, F.; Marzano, C. Advances in Copper Complexes as Anticancer Agents. *Chem. Rev.* **2014**, *114*, 815–862. [\[CrossRef\]](#)
53. Panova, E.V.; Voronina, J.K.; Safin, D.A. Copper(II) Chelates of Schiff Bases Enriched with Aliphatic Fragments: Synthesis, Crystal Structure, In Silico Studies of ADMET Properties and a Potency against a Series of SARS-CoV-2 Proteins. *Pharmaceuticals* **2023**, *16*, 286. [\[CrossRef\]](#)
54. Mohan, N.; Vidhya, C.V.; Suni, V.; Ameer, J.M.; Kasoju, N.; Mohanan, P.V.; Sreejith, S.S.; Kurup, M.R.P. Copper(II) salen-based complexes as potential anticancer agents. *New J. Chem.* **2022**, *46*, 12540–12550. [\[CrossRef\]](#)
55. Yusuf, T.L.; Oladipo, S.D.; Zamisa, S.; Kumalo, H.M.; Lawal, I.A.; Lawal, M.M.; Mabuba, N. Design of New Schiff-Base Copper(II) Complexes: Synthesis, Crystal Structures, DFT Study, and Binding Potency toward Cytochrome P450 3A4. *ACS Omega* **2021**, *6*, 13704–13718. [\[CrossRef\]](#) [\[PubMed\]](#)
56. Kargar, H.; Behjatmanesh-Ardakani, R.; Torabi, V.; Sarvian, A.; Kazemi, Z.; Chavoshpour-Natanzi, Z.; Mirkhani, V.; Sahraei, A.; Tahir, M.N.; Ashfaq, M. Novel copper(II) and zinc(II) complexes of halogenated bidentate N,O-donor Schiff base ligands: Synthesis, characterization, crystal structures, DNA binding, molecular docking, DFT and TD-DFT computational studies. *Inorg. Chim. Acta* **2021**, *514*, 120004. [\[CrossRef\]](#)
57. Guo, Y.N.; Hu, X.B.; Zhang, X.L.; Pu, X.H.; Wang, Y. The synthesis of a Cu(II) Schiff base complex using a bidentate N₂O₂ donor ligand: Crystal structure, photophysical properties, and antibacterial activities. *RSC Adv.* **2019**, *9*, 41737–41744. [\[CrossRef\]](#)
58. Lian, W.J.; Wang, X.T.; Xie, C.Z.; Tian, H.; Song, X.Q.; Pan, H.T.; Qiao, X.; Xu, J.Y. Mixed-ligand copper(II) Schiff base complexes: The role of the co-ligand in DNA binding, DNA cleavage, protein binding and cytotoxicity. *Dalton Trans.* **2016**, *45*, 9073–9087. [\[CrossRef\]](#) [\[PubMed\]](#)
59. Ei-Sherif, A.A.; Eldebss, T.M.A. Synthesis, spectral characterization, solution equilibria, in vitro antibacterial and cytotoxic activities of Cu(II), Ni(II), Mn(II), Co(II) and Zn(II) complexes with Schiff base derived from 5-bromosalicylaldehyde and 2-aminomethylthiophene. *Spectrochim. Acta Part A* **2011**, *79*, 1803–1814. [\[CrossRef\]](#)
60. Li, Y.P.; Wu, Y.B.; Zhao, J.; Yang, P. DNA-binding and cleavage studies of novel binuclear copper(II) complex with 1,1'-dimethyl-2,2'-biimidazole ligand. *J. Inorg. Biochem.* **2007**, *101*, 283–290. [\[CrossRef\]](#) [\[PubMed\]](#)
61. Lv, J.; Liu, T.T.; Cai, S.L.; Wang, X.; Liu, L.; Wang, Y.M. Synthesis, structure and biological activity of cobalt(II) and copper(II) complexes of valine-derived Schiff bases. *J. Inorg. Biochem.* **2006**, *100*, 1888–1896. [\[CrossRef\]](#)
62. Costamagna, J.; Ferraudi, G.; Matsuhira, B.; Campos-Vallette, M.; Canales, J.; Villagrán, M.; Vargas, J.; Aguirre, M.J. Complexes of macrocycles with pendant arms as models for biological molecules. *Coord. Chem. Rev.* **2000**, *196*, 125–164. [\[CrossRef\]](#)
63. Lei, Y.; Yang, Q.W.; Hu, Z.H.; Wang, S. Synthesis, structural studies and antimicrobial activity of copper(II) complexes derived from 2,4-difluoro-6-(((2-(pyrrolidin-1-yl)ethyl)imino) methyl)phenol. *Polyhedron* **2024**, *259*, 117071. [\[CrossRef\]](#)
64. Sonawane, H.R.; Vibhute, B.T.; Aghav, B.D.; Deore, J.V.; Patil, S.K. Versatile applications of transition metal incorporating quinoline Schiff base metal complexes: An overview. *Eur. J. Med. Chem.* **2023**, *258*, 115549. [\[CrossRef\]](#) [\[PubMed\]](#)
65. Kumar, R.; Singh, A.A.; Kumar, U.; Jain, P.; Sharma, A.K.; Kant, C.; Faizi, M.S.H. Recent advances in synthesis of heterocyclic Schiff base transition metal complexes and their antimicrobial activities especially antibacterial and antifungal. *J. Mol. Struct.* **2023**, *1294*, 136346. [\[CrossRef\]](#)
66. Devi, J.; Sharma, S.; Kumar, S.; Kumar, B.; Kumar, D.; Jindal, D.K.; Das, S. Synthesis, characterization, in vitro antimicrobial and cytotoxic studies of Co(II), Ni(II), Cu(II), and Zn(II) complexes obtained from Schiff base ligands of 1, 2, 3, 4-tetrahydro-naphthalen-1-ylamine. *Appl. Organomet. Chem.* **2022**, *36*, e6760. [\[CrossRef\]](#)
67. Peewasan, K.; Merkel, M.P.; Zarschler, K.; Stephan, H.; Anson, C.E.; Powell, A.K. Tetranuclear Cu(II)-chiral complexes: Synthesis, characterization and biological activity. *RSC Adv.* **2019**, *9*, 24087–24091. [\[CrossRef\]](#) [\[PubMed\]](#)
68. Dar, O.A.; Lone, S.A.; Malik, M.A.; Wani, M.Y.; Ahmad, A.; Hashmi, A.A. New transition metal complexes with a pendent indole ring: Insights into the antifungal activity and mode of action. *RSC Adv.* **2019**, *9*, 15151–15157. [\[CrossRef\]](#)
69. Kargar, H.; Aghaei-Meybodi, F.; Behjatmanesh-Ardakani, R.; Elahifard, M.R.; Torabi, V.; Fallah-Mehrjardi, M.; Tahir, M.N.; Ashfaq, M.; Munawar, K.S. Synthesis, crystal structure, theoretical calculation, spectroscopic and antibacterial activity studies of copper(II) complexes bearing bidentate Schiff base ligands derived from 4-aminoantipyrine: Influence of substitutions on antibacterial activity. *J. Mol. Struct.* **2021**, *1230*, 129908. [\[CrossRef\]](#)
70. Kargar, H.; Aghaei-Meybodi, F.; Elahifard, M.R.; Tahir, M.N.; Ashfaq, M.; Munawar, K.S. Some new Cu(II) complexes containing O,N-donor Schiff base ligands derived from 4-aminoantipyrine: Synthesis, characterization, crystal structure and substitution effect on antimicrobial activity. *J. Coord. Chem.* **2021**, *74*, 1534–1549. [\[CrossRef\]](#)

71. Alturiqi, A.S.; Alaghaz, A.; Zayed, M.E.; Ammar, R.A. Synthesis, characterization, biological activity, and corrosion inhibition in acid medium of unsymmetrical tetradentate N_2O_2 Schiff base complexes. *J. Chin. Chem. Soc.* **2018**, *65*, 1060–1074. [\[CrossRef\]](#)
72. Regojevic, M.S.; Zoric, M.Z.; Radnovic, N.D.; Bogdanovic, M.G.; Holló, B.B.; Rodic, M.V.; Raievic, V.; Borisev, I.D.; Vojinovic-Jesic, L.S.; Hozjan, M.; et al. Anion-directed synthesis of copper(I/II) complexes with a Schiff base derived from 2-(diphenylphosphino)benzaldehyde and aminoguanidine. *J. Mol. Struct.* **2025**, *1336*, 14. [\[CrossRef\]](#)
73. Khalaji, A.D.; Weil, M.; Hadadzadeh, H.; Daryanavard, M. Two different 1D-chains in the structures of the copper(I) coordination polymers based on bidentate Schiff-base building units and thiocyanate anions as bridging ligands. *Inorg. Chim. Acta* **2009**, *362*, 4837–4842. [\[CrossRef\]](#)
74. Morshedi, M.; Amirnasr, M.; Triki, S.; Khalaji, A.D. New (NS)₂ Schiff base with a flexible spacer: Synthesis and structural characterization of its first coordination polymer $[Cu_2(I-I)_2(I-(thio)2dapte)]_n$ (1). *Inorg. Chim. Acta* **2009**, *362*, 1637–1640. [\[CrossRef\]](#)
75. Ferraro, V.; Fuhr, O.; Bizzarri, C.; Braese, S. Substituted Pyrrole-based Schiff Bases: Effect on the Luminescence of Neutral Heteroleptic Cu(I) Complexes. *Eur. J. Inorg. Chem.* **2024**, *27*, e202400080. [\[CrossRef\]](#)
76. Crestani, M.G.; Manbeck, G.F.; Brennessel, W.W.; McCormick, T.M.; Eisenberg, R. Synthesis and Characterization of Neutral Luminescent Diphosphine Pyrrole- and Indole-Aldimine Copper(I) Complexes. *Inorg. Chem.* **2011**, *50*, 7172–7188. [\[CrossRef\]](#)
77. Lv, J.; Wu, X.Y.; Wang, R.; Wu, Y.Q.; Xu, S.X.; Zhao, F.; Wang, Y.B. Schiff base-type Cu(I) complexes containing naphthylpyridyl-methanimine ligands featuring higher light-absorption capability: Synthesis, structures, and photophysical properties. *Polyhedron* **2022**, *224*, 116002. [\[CrossRef\]](#)
78. Lv, J.; Lu, Y.F.; Wang, J.L.; Zhao, F.; Wang, Y.B.; He, H.F.; Wu, Y.Q. Schiff base-type copper(I) complexes exhibiting high molar extinction coefficients: Synthesis, characterization and DFT studies. *J. Mol. Struct.* **2022**, *1249*, 131638. [\[CrossRef\]](#)
79. Lv, J.; Li, Q.Q.; Wang, J.L.; Xu, S.X.; Zhao, F.; He, H.F.; Wang, Y.B. Orange-red emissive Cu(I) complexes bearing Schiff base ligands: Synthesis, structures, and photophysical properties. *J. Mol. Struct.* **2022**, *1252*, 132180. [\[CrossRef\]](#)
80. Klasen, H.J. A historical review of the use of silver in the treatment of burns. II. Renewed interest for silver. *Burns* **2000**, *26*, 131–138. [\[CrossRef\]](#) [\[PubMed\]](#)
81. Cai, L.; Huang, Y.Q.; Duan, Y.Y.; Liu, Q.; Xu, Q.L.; Jia, J.; Wang, J.M.; Tong, Q.; Luo, P.P.; Wen, Y.J.; et al. Schiff-base silver nanocomplexes formation on natural biopolymer coated mesoporous silica contributed to the improved curative effect on infectious microbes. *Nano Res.* **2021**, *14*, 2735–2748. [\[CrossRef\]](#)
82. Azócar, M.I.; Gómez, G.; Levín, P.; Paez, M.; Muñoz, H.; Dinamarca, N. Review: Antibacterial behavior of carboxylate silver(I) complexes. *J. Coord. Chem.* **2014**, *67*, 3840–3853. [\[CrossRef\]](#)
83. Nomiya, K.; Tsuda, K.; Sudoh, T.; Oda, M. Ag(I)-N bond-containing compound showing wide spectra in effective antimicrobial activities: Polymeric silver(I) imidazolate. *J. Inorg. Biochem.* **1997**, *68*, 39–44. [\[CrossRef\]](#)
84. Khan, E.; Hanif, M.; Akhtar, M.S. Schiff bases and their metal complexes with biologically compatible metal ions; biological importance, recent trends and future hopes. *Rev. Inorg. Chem.* **2022**, *42*, 307–325. [\[CrossRef\]](#)
85. Njogu, E.M.; Omondi, B.; Nyamori, V.O. Silver(I)-pyridinyl Schiff base complexes: Synthesis, characterisation and antimicrobial studies. *J. Mol. Struct.* **2017**, *1135*, 118–128. [\[CrossRef\]](#)
86. Adeleke, A.A.; Oladipo, S.D.; Zamisa, S.J.; Sanusi, I.A.; Omondi, B. DNA/BSA binding studies and in vitro anticancer and antibacterial studies of isoelectronic Cu(I)- and Ag(I)-pyridinyl Schiff base complexes incorporating triphenylphosphine as co-ligands. *Inorg. Chim. Acta* **2023**, *558*, 121760. [\[CrossRef\]](#)
87. Raczkuk, E.; Dmochowska, B.; Samaszko-Fiartek, J.; Madaj, J. Different Schiff Bases-Structure, Importance and Classification. *Molecules* **2022**, *27*, 787. [\[CrossRef\]](#) [\[PubMed\]](#)
88. Ren, M.; Xu, Z.L.; Bao, S.S.; Wang, T.T.; Zheng, Z.H.; Ferreira, R.A.S.; Zheng, L.M.; Carlos, L.D. Lanthanide salen-type complexes exhibiting single ion magnet and photoluminescent properties. *Dalton Trans.* **2016**, *45*, 2974–2982. [\[CrossRef\]](#)
89. Kitamura, F.; Sawaguchi, K.; Mori, A.; Takagi, S.; Suzuki, T.; Kobayashi, A.; Kato, M.; Nakajima, K. Coordination Structure Conversion of Hydrazone-Palladium(II) Complexes in the Solid State and in Solution. *Inorg. Chem.* **2015**, *54*, 8436–8448. [\[CrossRef\]](#) [\[PubMed\]](#)
90. Chew, S.T.; Lo, K.M.; Sinniah, S.K.; Sim, K.S.; Tan, K.W. Synthesis, characterization and biological evaluation of cationic hydrazone copper complexes with diverse diimine co-ligands. *RSC Adv.* **2014**, *4*, 61232–61247. [\[CrossRef\]](#)
91. Su, W.; Qian, Q.Q.; Li, P.Y.; Lei, X.L.; Xiao, Q.; Huang, S.; Huang, C.S.; Cui, J.G. Synthesis, Characterization, and Anticancer Activity of a Series of Ketone- N^4 -Substituted Thiosemicarbazones and Their Ruthenium(II) Arene Complexes. *Inorg. Chem.* **2013**, *52*, 12440–12449. [\[CrossRef\]](#)
92. Whiteoak, C.J.; Salassa, G.; Kleij, A.W. Recent advances with π -conjugated salen systems. *Chem. Soc. Rev.* **2012**, *41*, 622–631. [\[CrossRef\]](#)
93. Krishnamoorthy, P.; Sathyadevi, P.; Butorac, R.R.; Cowley, A.H.; Bhuvanesh, N.S.P.; Dharmaraj, N. Copper(I) and nickel(II) complexes with 1:1 vs. 1:2 coordination of ferrocenyl hydrazone ligands: Do the geometry and composition of complexes affect DNA binding/cleavage, protein binding, antioxidant and cytotoxic activities? *Dalton Trans.* **2012**, *41*, 4423–4436. [\[CrossRef\]](#)

94. Bagherzadeh, M.; Zare, M. Synthesis and characterization of NaY zeolite-encapsulated Mn-hydrazone Schiff base: An efficient and reusable catalyst for oxidation of olefins. *J. Coord. Chem.* **2012**, *65*, 4054–4066. [\[CrossRef\]](#)
95. Chellan, P.; Land, K.M.; Shokar, A.; Au, A.; An, S.H.; Clavel, C.M.; Dyson, P.J.; de Kock, C.; Smith, P.J.; Chibale, K.; et al. Exploring the Versatility of Cycloplatinated Thiosemicarbazones as Antitumor and Antiparasitic Agents. *Organometallics* **2012**, *31*, 5791–5799. [\[CrossRef\]](#)
96. Prabhakaran, R.; Kalaivani, P.; Poornima, P.; Dallemer, F.; Paramaguru, G.; Padma, V.V.; Renganathan, R.; Huang, R.; Natarajan, K. One pot synthesis of structurally different mono and dimeric Ni(II) thiosemicarbazone complexes and *N*-arylation on a coordinated ligand: A comparative biological study. *Dalton Trans.* **2012**, *41*, 9323–9336. [\[CrossRef\]](#)
97. Minkin, V.I.; Tsukanov, A.V.; Dubonosov, A.D.; Bren, V.A. Tautomeric Schiff bases: Iono-, solvato-, thermo- and photochromism. *J. Mol. Struct.* **2011**, *998*, 179–191. [\[CrossRef\]](#)
98. Hansen, P.E.; Filarowski, A. Characterisation of the PT-form of *o*-hydroxy acylarornatic Schiff bases by NMR spectroscopy and DFT calculations. *J. Mol. Struct.* **2004**, *707*, 69–75. [\[CrossRef\]](#)
99. Dominiak, P.M.; Grech, E.; Barr, G.; Teat, S.; Mallinson, P.; Wozniak, K. Neutral and ionic hydrogen bonding in Schiff bases. *Chem. Eur. J.* **2003**, *9*, 963–970. [\[CrossRef\]](#) [\[PubMed\]](#)
100. Król-Starzomska, I.; Filarowski, A.; Rospenk, M.; Koll, A.; Melikova, S. Proton transfer equilibria in Schiff bases with steric repulsion. *J. Phys. Chem. A* **2004**, *108*, 2131–2138. [\[CrossRef\]](#)
101. Filarowski, A.; Glowia, T.; Koll, A. Strengthening of the intramolecular O···H···N hydrogen bonds in Schiff bases as a result of steric repulsion. *J. Mol. Struct.* **1999**, *484*, 75–89. [\[CrossRef\]](#)
102. Jinno, S.; Senoo, T.; Mori, K. Access to *ortho*-Hydroxyphenyl Ketimines via Imine Anion-Mediated Smiles Rearrangement. *Org. Lett.* **2022**, *24*, 4140–4144. [\[CrossRef\]](#)
103. Guerrero-Corella, A.; Esteban, F.; Iniesta, M.; Martín-Somer, A.; Parra, M.; Díaz-Tendero, S.; Fraile, A.; Alemán, J. 2-Hydroxybenzophenone as a Chemical Auxiliary for the Activation of Ketiminoesters for Highly Enantioselective Addition to Nitroalkenes under Bifunctional Catalysis. *Angew. Chem. Int. Ed.* **2018**, *57*, 5350–5354. [\[CrossRef\]](#)
104. Al-Qaisi, F.; Genjang, N.; Nieger, M.; Repo, T. Synthesis, structure and catalytic activity of bis(phenoxyiminato)iron(III) complexes in coupling reaction of CO₂ and epoxides. *Inorg. Chim. Acta* **2016**, *442*, 81–85. [\[CrossRef\]](#)
105. Sibaoui, A.; Ryan, P.; Axenov, K.V.; Sundberg, M.R.; Leskelä, M.; Repo, T. Efficient coupling of CO₂ and epoxides with bis(phenoxyiminato) cobalt(III)/Lewis base catalysts. *J. Mol. Catal. A Chem.* **2009**, *312*, 87–91. [\[CrossRef\]](#)
106. Marcazzan, P.; Patrick, B.O.; James, B.R. Catalyst poisoning in catalyzed imine hydrogenation: A novel zwitterionic Rh(I)/*o*-hydroxy-substituted imine complex. *J. Mol. Catal. A Chem.* **2006**, *257*, 26–30. [\[CrossRef\]](#)
107. Cimarelli, C.; Palmieri, G.; Volpini, E. Synthesis of enantiopure 2-aminoalkylphenols by stereoselective addition of Grignard reagents to chiral 2-imidoylphenols. *Tetrahedron Asymmetry* **2002**, *13*, 2011–2018. [\[CrossRef\]](#)
108. Mondal, B.; Chakraborty, S.; Munshi, P.; Walawalkar, M.G.; Lahiri, G.K. Ruthenium(II)/-(III) terpyridine complexes incorporating imine functionalities. Synthesis, structure, spectroscopic and electrochemical properties. *J. Chem. Soc. Dalton Trans.* **2000**, 2327–2335. [\[CrossRef\]](#)
109. Keerthi, K.D.; Santra, B.K.; Lahiri, G.K. Ruthenium(II) bipyridine complexes with modified phenolic Schiff base ligands. Synthesis, spectroscopic characterization and redox properties. *Polyhedron* **1998**, *17*, 1387–1396. [\[CrossRef\]](#)
110. Choudhary, N.; Hughes, D.L.; Kleinkes, U.; Larkworthy, L.F.; Leigh, G.J.; Maiwald, M.; Marmion, C.J.; Sanders, J.R.; Smith, G.W.; Sudbrake, C. New tetradentate Schiff bases, their oxovanadium(IV) complexes, and some complexes of bidentate Schiff bases with vanadium(III). *Polyhedron* **1997**, *16*, 1517–1528. [\[CrossRef\]](#)
111. Pellei, M.; Santini, C.; Bagnarelli, L.; Caviglia, M.; Sgarbossa, P.; De Franco, M.; Zancato, M.; Marzano, C.; Gandin, V. Novel Silver Complexes Based on Phosphanes and Ester Derivatives of Bis(pyrazol-1-yl)acetate Ligands Targeting TrxR: New Promising Chemotherapeutic Tools Relevant to SCLC Management. *Int. J. Mol. Sci.* **2023**, *24*, 4091. [\[CrossRef\]](#)
112. Del Bello, F.; Pellei, M.; Bagnarelli, L.; Santini, C.; Giorgioni, G.; Piergentili, A.; Quaglia, W.; Battocchio, C.; Iucci, G.; Schiesaro, I.; et al. Cu(I) and Cu(II) Complexes Based on Lonidamine-Conjugated Ligands Designed to Promote Synergistic Antitumor Effects. *Inorg. Chem.* **2022**, *61*, 4919–4937. [\[CrossRef\]](#)
113. Pellei, M.; Bagnarelli, L.; Luciani, L.; Del Bello, F.; Giorgioni, G.; Piergentili, A.; Quaglia, W.; De Franco, M.; Gandin, V.; Marzano, C.; et al. Synthesis and Cytotoxic Activity Evaluation of New Cu(I) Complexes of Bis(pyrazol-1-yl) Acetate Ligands Functionalized with an NMDA Receptor Antagonist. *Int. J. Mol. Sci.* **2020**, *21*, 2616. [\[CrossRef\]](#)
114. Morelli, M.B.; Amantini, C.; Santoni, G.; Pellei, M.; Santini, C.; Cimarelli, C.; Marcantoni, E.; Petrini, M.; Del Bello, F.; Giorgioni, G.; et al. Novel antitumor copper(II) complexes designed to act through synergistic mechanisms of action, due to the presence of an NMDA receptor ligand and copper in the same chemical entity. *New J. Chem.* **2018**, *42*, 11878–11887. [\[CrossRef\]](#)
115. Gandin, V.; Ceresa, C.; Esposito, G.; Indraccolo, S.; Porchia, M.; Tisato, F.; Santini, C.; Pellei, M.; Marzano, C. Therapeutic potential of the phosphino Cu(I) complex (HydroCuP) in the treatment of solid tumors. *Sci. Rep.* **2017**, *7*, 13936. [\[CrossRef\]](#)

116. Tisato, F.; Marzano, C.; Peruzzo, V.; Tegoni, M.; Giorgetti, M.; Damjanovic, M.; Trapananti, A.; Bagno, A.; Santini, C.; Pellei, M.; et al. Insights into the cytotoxic activity of the phosphane copper(I) complex Cu(thp)(4) PF₆. *J. Inorg. Biochem.* **2016**, *165*, 80–91. [\[CrossRef\]](#) [\[PubMed\]](#)
117. Papini, G.; Bandoli, G.; Dolmella, A.; Gioia Lobbia, G.; Pellei, M.; Santini, C. New homoleptic carbene transfer ligands and related coinage metal complexes. *Inorg. Chem. Commun.* **2008**, *11*, 1103–1106. [\[CrossRef\]](#)
118. Räisänen, M.T.; Elo, P.; Kettunen, M.; Klinga, M.; Leskelä, M.; Repo, T. Practical method for 2-hydroxyphenylketimine synthesis. *Synth. Commun.* **2007**, *37*, 1765–1777. [\[CrossRef\]](#)
119. Cimarelli, C.; Palmieri, G.; Volpini, E. An improved solvent-free preparation of 2-imidoylphenols. *Org. Prep. Proced. Int.* **2001**, *33*, 369–371. [\[CrossRef\]](#)
120. Cimarelli, C.; Palmieri, G. Alkylation of dianions derived from 2-(1-iminoalkyl) phenols: Synthesis of functionalized 2-acyl phenols. *Tetrahedron* **1998**, *54*, 15711–15720. [\[CrossRef\]](#)
121. Filarowski, A.; Koll, A.; Głowiak, T. Steric Modification of the Intramolecular Hydrogen Bond in 2-(Methylimino-phenyl-methyl)-phenols. *Monatshefte Chem.* **1999**, *130*, 1097–1108. [\[CrossRef\]](#)
122. Mihaylov, M.Y.; Zdravkova, V.R.; Ivanova, E.Z.; Aleksandrov, H.A.; St Petkov, P.; Vayssilov, G.N.; Hadjiivanov, K.I. Infrared spectra of surface nitrates: Revision of the current opinions based on the case study of ceria. *J. Catal.* **2021**, *394*, 245–258. [\[CrossRef\]](#)
123. Nakamoto, K. Applications in Coordination Chemistry. In *Infrared and Raman Spectra of Inorganic and Coordination Compounds: Part B: Applications in Coordination, Organometallic, and Bioinorganic Chemistry*; John Wiley & Sons: Hoboken, NJ, USA, 2008; pp. 1–273.
124. Effendy; Healy, P.C.; Marchetti, F.; Pettinari, C.; Pettinari, R.; Tombesi, A.; Skelton, B.W.; White, A.H. Synthesis and structural characterization of some 1:1 and 1:2 adducts of silver(I) salts with hindered Pmes₃, PPhmes₂ and PPh₂mes bases (Ph = phenyl, mes = 2,4,6-trimethylphenyl). *Inorg. Chim. Acta* **2022**, *535*, 120857. [\[CrossRef\]](#)
125. Meijboom, R.; Bowen, R.J.; Berners-Price, S.J. Coordination complexes of silver(I) with tertiary phosphine and related ligands. *Coord. Chem. Rev.* **2009**, *253*, 325–342. [\[CrossRef\]](#)
126. Barron, P.F.; Dyason, J.C.; Healy, P.C.; Engelhardt, L.M.; Skelton, B.W.; White, A.H. Lewis Base Adducts of Group 11 Metal Compounds. Part 24. Co-ordination of Triphenylphosphine with Silver Nitrate. A Solid-state Cross-polarization Magic Angle Spinning ³¹P Nuclear Magnetic Resonance, Crystal Structure, and Infrared Spectroscopic Study of Ag(PPh₃)_nNO₃ (n = 1–4). *J. Chem. Soc.-Dalton Trans.* **1986**, *9*, 1965–1970.
127. Pellei, M.; Del Gobbo, J.; Caviglia, M.; Karade, D.V.; Gandin, V.; Marzano, C.; Poyil, A.N.; Dias, H.V.R.; Santini, C. Synthesis and cytotoxicity studies of Cu(I) and Ag(I) complexes based on sterically hindered β-diketonates with different degrees of fluorination. *Dalton Trans.* **2023**, *52*, 12098–12111. [\[CrossRef\]](#) [\[PubMed\]](#)
128. Dias, H.V.R.; Flores, J.A.; Pellei, M.; Morresi, B.; Gioia Lobbia, G.; Singh, S.; Kobayashi, Y.; Yousufuddin, M.; Santini, C. Silver(I) and copper(I) complexes supported by fully fluorinated 1,3,5-triazapentadienyl ligands. *Dalton Trans.* **2011**, *40*, 8569–8580. [\[CrossRef\]](#)
129. Pellei, M.; Alidori, S.; Papini, G.; Gioia Lobbia, G.; Gorden, J.D.; Dias, H.V.R.; Santini, C. Silver(I)-organophosphane complexes of electron withdrawing CF₃- or NO₂-substituted scorpionate ligands. *Dalton Trans.* **2007**, 4845–4853. [\[CrossRef\]](#)
130. Dias, H.V.R.; Alidori, S.; Gioia Lobbia, G.; Papini, G.; Pellei, M.; Santini, C. Small Scorpionate Ligands: Silver(I)-Organophosphane Complexes of 5-CF₃-Substituted Scorpionate Ligand Combining a B–H⋯Ag Coordination Motif. *Inorg. Chem.* **2007**, *46*, 9708–9714. [\[CrossRef\]](#)
131. Okuniewski, A.; Rosiak, D.; Chojnacki, J.; Becker, B. Coordination polymers and molecular structures among complexes of mercury(II) halides with selected 1-benzoylthioureas. *Polyhedron* **2015**, *90*, 47–57. [\[CrossRef\]](#)
132. Yang, L.; Powell, D.R.; Houser, R.P. Structural variation in copper(I) complexes with pyridylmethylamide ligands: Structural analysis with a new four-coordinate geometry index, τ₄. *Dalton Trans.* **2007**, *9*, 955–964. [\[CrossRef\]](#)
133. Allen, F.H. The Cambridge Structural Database: A quarter of a million crystal structures and rising. *Acta Cryst.* **2002**, *B58*, 380–388. [\[CrossRef\]](#)
134. Wang, D.J.; Fan, L.; Wang, G.H. Crystal structure of N-(diphenylmethylene)diphenylmethanamine, C₂₆H₂₁N. *Z. Krist.-New Cryst. Struct.* **2009**, *224*, 186–188.
135. Liu, X.L.; Gao, A.; Ding, L.; Xu, J.; Zhao, B.G. Aminative Umpolung Synthesis of Aryl Vicinal Diamines from Aromatic Aldehydes. *Org. Lett.* **2014**, *16*, 2118–2121. [\[CrossRef\]](#) [\[PubMed\]](#)
136. Vorontsova, N.V.; Bystrova, G.S.; Antonov, D.Y.; Vologzhanina, A.V.; Godovikov, I.A.; Il'in, M.M. Novel ligands based on bromosubstituted hydroxycarbonyl 2.2 paracyclophane derivatives: Synthesis and application in asymmetric catalysis. *Tetrahedron Asymmetry* **2010**, *21*, 731–738. [\[CrossRef\]](#)
137. Blackwell, J.M.; Piers, W.E.; Parvez, M.; McDonald, R. Solution and solid-state characteristics of imine adducts with tris(pentafluorophenyl)borane. *Organometallics* **2002**, *21*, 1400–1407. [\[CrossRef\]](#)

138. Rozenberg, V.; Danilova, T.Y.; Sergeeva, E.; Vorontsov, E.; Starikova, Z.; Lysenko, K.; Belokon', Y. Regioselective Fries Rearrangement and Friedel–Crafts Acylation as Efficient Routes to Novel Enantiomerically Enriched ortho-Acylhydroxy [2.2]paracyclophanes. *Eur. J. Org. Chem.* **2000**, *2000*, 3295–3303. [\[CrossRef\]](#)
139. Ito, M.; Kasuga, N.C.; Matsuse, R.; Hirotsu, M. Crystal structures and circular dichroism of {2,20-[(1*S*,2*S*)-1,2-diphenylethane-1,2-diylbis(nitrilo-phenylmethanylylidene)]diphenolato} nickel(II) and its ethanol solvate. *Acta Cryst.* **2024**, *E80*, 1259–1265.
140. Hirotsu, M.; Kuwamura, N.; Kinoshita, I.; Kojima, M.; Yoshikawa, Y.; Ueno, K. Steric, geometrical and solvent effects on redox potentials in salen-type copper(II) complexes. *Dalton Trans.* **2009**, 7678–7683. [\[CrossRef\]](#)
141. Hirotsu, M.; Kojima, M.; Nakajima, K.; Kashino, S.; Yoshikawa, Y. Stereochemistry and electrochemistry of cobalt(II) and cobalt(III) complexes containing optically active tetradentate Schiff base ligands. *Bull. Chem. Soc. Jpn.* **1996**, *69*, 2549–2557. [\[CrossRef\]](#)
142. Hirotsu, M.; Nakajima, K.; Kojima, M.; Yoshikawa, Y. Manganese(III) Complexes Containing Optically Active Tetradentate Schiff Base Ligands. Effect of Phenyl Substituents. *Inorg. Chem.* **1995**, *34*, 6173–6178. [\[CrossRef\]](#)
143. Hirotsu, M.; Kojima, M.; Nakajima, K.; Kashino, S.; Yoshikawa, Y. Steric Control of Redox Potentials of Cobalt(II) Schiff Base Complexes with Phenyl Substituents. *Chem. Lett.* **1994**, *23*, 2183–2186. [\[CrossRef\]](#)
144. Cifuentes-Vaca, O.L.; Andrades-Lagos, J.; Campanini-Salinas, J.; Laguna, A.; Vásquez-Velásquez, D.; Gimeno, M.C. Silver(I) and copper(I) complexes with a Schiff base derived from 2-aminofluorene with promising antibacterial activity. *Inorg. Chim. Acta* **2019**, *489*, 275–279. [\[CrossRef\]](#)
145. Berthon, G. Critical evaluation of the stability constants of metal complexes of amino acids* with polar side chains (Technical report). *Pure Appl. Chem.* **1995**, *67*, 1117–1240. [\[CrossRef\]](#)
146. Kumar, M.; Singh, A.K.; Singh, S.; Singh, A.K.; Rao, P.K.; Yadav, R.K.; Singh, A.P.; Tripathi, U.N. Exploration of iron(III) complexes with bidentate N, O-donor Schiff base ligands through synthesis, characterization, DFT, and antibacterial studies. *J. Mol. Struct.* **2025**, *1319*, 139496. [\[CrossRef\]](#)
147. Salah, N.; Adly, O.M.I.; Ibrahim, M.A.; Abdelaziz, M.; Abdelrhman, E.M. New Metal Complexes Incorporating Schiff Base Ligand Based on Pyridine Moiety: Synthesis, Spectral Characterization, DFT, Biological Evaluation, and Molecular Docking. *Appl. Organomet. Chem.* **2025**, *39*, e7751. [\[CrossRef\]](#)
148. Oladipo, S.D.; Mocktar, C.; Omondi, B. In vitro biological studies of heteroleptic Ag(I) and Cu(I) unsymmetrical N,N'-diarylformamidinium dithiocarbamate phosphine complexes; the effect of the metal center. *Arab. J. Chem.* **2020**, *13*, 6379–6394. [\[CrossRef\]](#)
149. Reddy, T.S.; Privér, S.H.; Ojha, R.; Mirzadeh, N.; Velma, G.R.; Jakku, R.; Hosseinejad, T.; Luwor, R.; Ramakrishna, S.; Wlodkowic, D.; et al. Gold(I) complexes of the type [AuL{κC-2-C₆H₄P(S)Ph₂}] [L = PTA, PPh₃, PPh₂(C₆H₄-3-SO₃Na) and PPh₂(2-py)]: Synthesis, characterisation, crystal structures, and In Vitro and In Vivo anticancer properties. *Eur. J. Med. Chem.* **2025**, *281*, 117007. [\[CrossRef\]](#) [\[PubMed\]](#)
150. Singh, K.; Singh, V.K.; Mishra, R.; Sharma, A.; Pandey, A.; Srivastava, S.K.; Chaurasia, H. Design, Synthesis, DFT, docking Studies, and antimicrobial evaluation of novel benzimidazole containing sulphonamide derivatives. *Bioorg. Chem.* **2024**, *149*, 107473. [\[CrossRef\]](#)
151. Yan, Y.; Xia, X.X.; Fatima, A.; Zhang, L.; Yuan, G.J.; Lian, F.X.; Wang, Y. Antibacterial Activity and Mechanisms of Plant Flavonoids against Gram-Negative Bacteria Based on the Antibacterial Statistical Model. *Pharmaceuticals* **2024**, *17*, 292. [\[CrossRef\]](#)
152. Hasan, A.; Varna, D.; Chakraborty, I.; Angaridis, P.A.; Raptis, R.G. Synthesis, structure and antibacterial properties of a mononuclear Ag(I) complex, [Ag(OBz)(PTA)₂] (OBz = benzoate, PTA = 1,3,5-triaza-7-phospadamantane). *Results Chem.* **2022**, *4*, 100580. [\[CrossRef\]](#)
153. Pervaiz, M.; Sadiq, A.; Sadiq, S.; Saeed, Z.; Imran, M.; Younas, U.; Bukhari, S.M.; Khan, R.R.M.; Rashid, A.; Adnan, A. Design and synthesis of Schiff base Homobimetallic-Complexes as promising antimicrobial agents. *Inorg. Chem. Commun.* **2022**, *137*, 109206. [\[CrossRef\]](#)
154. Ejidike, I.P. Cu(II) Complexes of 4-[(1*E*)-N-{2-[(*Z*)-Benzylidene-amino]ethyl}ethanimidoyl]benzene-1,3-diol Schiff Base: Synthesis, Spectroscopic, In-Vitro Antioxidant, Antifungal and Antibacterial Studies. *Molecules* **2018**, *23*, 1581. [\[CrossRef\]](#)
155. Calu, L.; Badea, M.; Korosin, N.C.; Chifiriuc, M.C.; Bleotu, C.; Stanica, N.; Silvestro, L.; Maurer, M.; Olar, R. Spectral, thermal and biological characterization of complexes with a Schiff base bearing triazole moiety as potential antimicrobial species. *J. Therm. Anal. Calorim.* **2018**, *134*, 1839–1850. [\[CrossRef\]](#)
156. Zhang, Y.B.; Liu, Q.; Jing, H.R.; Cai, Y.J.; Wang, Q.; Li, Y.G. Synthesis, characterization, and antimicrobial activity of two Schiff base silver(I) complexes derived from 4-carboxybenzaldehyde. *J. Coord. Chem.* **2017**, *70*, 1066–1076. [\[CrossRef\]](#)
157. *CrysAlisPro Versions 1.171.43.141a*; Rigaku Oxford Diffraction: Oxford, UK, 2024.
158. Dolomanov, O.V.; Bourhis, L.J.; Gildea, R.J.; Howard, J.A.K.; Puschmann, H. OLEX2: A complete structure solution, refinement and analysis program. *J. Appl. Crystallogr.* **2009**, *42*, 339–341. [\[CrossRef\]](#)
159. Sheldrick, G.M. SHELXT—Integrated space-group and crystal-structure determination. *Acta Cryst.* **2015**, *A71*, 3–8. [\[CrossRef\]](#) [\[PubMed\]](#)
160. Sheldrick, G.M. Crystal structure refinement with SHELXL. *Acta Cryst.* **2015**, *C71*, 3–8.

161. Macrae, C.F.; Bruno, I.J.; Chisholm, J.A.; Edgington, P.R.; McCabe, P.; Pidcock, E.; Rodriguez-Monge, L.; Taylor, R.; van de Streek, J.; Wood, P.A. Mercury CSD 2.0—New features for the visualization and investigation of crystal structures. *J. Appl. Crystallogr.* **2008**, *41*, 466–470. [[CrossRef](#)]
162. Liu, J.M.; Guo, C.P.; Liu, Z.Z.; Cheng, F.; Zhang, S.; Zhang, Z.H. Simultaneous sterilization and biosensing of pathogenic bacteria via copper phthalocyanine-based COF embedded with Cu-N4 single atomic sites and silver nanoparticles. *Chem. Eng. J.* **2024**, *494*, 153139. [[CrossRef](#)]

Disclaimer/Publisher’s Note: The statements, opinions and data contained in all publications are solely those of the individual author(s) and contributor(s) and not of MDPI and/or the editor(s). MDPI and/or the editor(s) disclaim responsibility for any injury to people or property resulting from any ideas, methods, instructions or products referred to in the content.